Protein-protein interactions within the ciliary tip module depend on different functional domains and are disrupted by Joubert syndrome variants

Major research internship report of Donna Schweizer
Student number: 6462111
Masters program: Molecular and Cellular Life Sciences

Department of Cell biology, Utrecht University
Daily supervisor: Dr. Harriet Saunders
First examiner: Prof. Dr. Anna Akhmanova
Second examiner: Prof. Dr. Lukas Kapitein

27/12/2023

[ABSTRACT] Primary cilia are microtubule based organelles found on the surface of many eukaryotic cell types. They are involved in various signalling pathways, for example in hedgehog signalling. Defects to primary cilia underly a subset of disorders, together termed ciliopathies, including the neurodevelopmental disorder Joubert syndrome (1)**. Ciliary length is directly determined by axonemal microtubule length and is suggested to be crucial for proper cilia functioning, as ciliopathy patient-derived cells typically contain cilia with abnormal lengths** (2–4)**. A recent study characterized how proteins ARMC9, CCDC66, CEP104, mCrescerin1 and CSPP1, the core components of the ciliary tip module, directly affect microtubule dynamics through in vitro reconstitutions** (5,6)**. Unpublished cryo-ET data from our lab shows that these proteins form a single complex at microtubule plus ends. Yet the exact geometry of individual proteins within this complex and how interactions are facilitated remains unclear, especially when proteins are localized on opposite sides of the microtubule wall. In this study, we further map protein-protein interactions within the tip module. By performing multiple co-immunoprecipitations assays, we narrowed down interactions between (I)ARMC9 and mCrescerin1, (II) ARMC9 and CSPP1 and (III) CEP104 and mCrescerin1 to a specific functional domain or protein region and confirmed from literature that interaction of CEP104 with CCDC66 or CSPP1 is dependent on its jelly roll domain. Additionally, we showed that mutations linked to the ciliopathy Joubert syndrome affect ARMC9-mCrescerin1, CEP104-CCDC66 and CEP104-CSPP1 interactions, highlighting the biological relevance of protein-protein interactions within the tip module.**

Introduction

Primary cilia are highly specialized, microtubule-based organelles found as single protrusions on the surface of many eukaryotic cell types (7). They are immotile and function as key signalling centres by decoding a variety of mechanical and chemical stimuli (8). Primary cilia are for example involved in hedgehog and Wnt signalling and play a fundamental role during development and in homeostasis (4,9,10). The core of a primary cilium consists of the axoneme, a microtubule based structure, which provides structural support and serves as the track for intraflagellar transport motors (1–3). The axoneme is formed by a radial array of 9 A and B microtubule doublets, referred to as '9 + 0 architecture' (11). It nucleates from and is anchored to the cell by the basal body, a modified centriole (4,7). Post-translational modifications of axonemal microtubules, such as acetylation and glutamylation, contribute to axoneme stability (4). Axonemal microtubule dynamics are regulated at the ciliary tip, the region between the distal end of the axoneme and the ciliary membrane. The tip is also the site of remodelling of intraflagellar transport trains and hedgehog

signalling (7). Ciliopathies, a subset of genetic disorders, generally directly or indirectly affect cilia function or formation and in many cases compromise the structural integrity of the cilium (12). Ciliary length is directly determined by axonemal microtubule length (13). Ciliopathy patient-derived cells typically contain cilia of abnormal lengths, suggesting that ciliary and therefore axonemal microtubule length is essential for proper cilia function (2–4).

Although various proteins and pathways involved in the regulation of axoneme structure have been identified through genetic screens and in vivo cell biology studies, the molecular mechanisms behind the regulation of axonemal microtubules often remain elusive (5). Here, we focus on the recently identified ciliary tip module with the core components; ARMC9, CCDC66, CEP104, CSPP1 and TOGARAM1 (2,5). All proteins localize to the ciliary tip, are important for signalling and are known to interact with microtubules and with each other, suggesting they regulate axonemal microtubule length and dynamics (2,5,7,14–16). Depletion of any has been shown to result in shortened cilia and mutations in all but CCDC66 have been linked to the ciliopathy Joubert syndrome. Joubert syndrome (JBTS) is a rare developmental disorder, diagnosed by a specific malformation of the brain stem (molar tooth sign) and is additionally associated with hypotonia, ataxia and kidney and liver dysfunction (17). In a recent study, the exact molecular mechanism of action of the tip module, both individually as in various combinations, was characterized through in vitro reconstitutions of dynamic microtubules (5,6). However, it remains unclear how interactions between various tip module proteins are facilitated.

CEP104 contains one evolutionary conserved TOG domain which can bind tubulin (18,19). It plays an important role in ciliogenesis by counteracting the block of CP110 and CEP97 to allow centriole elongation and relocates from the mother centriole to the axoneme tip once cilia formation is initiated (15,18). CEP104 gets recruited to the microtubule plus end through interaction with EBs and has been shown to directly interact with CCDC66 and CSPP1 through an N-terminal jelly roll (JR) domain (5,15,16,19). Interaction between CEP104 and CSPP1 is required for Hedgehog signalling competent primary cilia and co-depletion of both CCDC66 or CSPP1 and CEP104 results in even shorter cilia in cells in comparison to depletion of these proteins individually (15,16,20–22). In vitro, CEP104 localizes to growing microtubule ends, potentiated by EB3, CCDC66 or CSPP1, and upon sufficient accumulation completely blocks further microtubule growth (5). CEP104 induced blocks can be counteracted by TOGARAM1(5).

TOGARAM1 contains four TOG domains (2,23). Depletion of TOGARAM1 or one of its homologues also leads to shorter cilia in cultured mammalian cells or model organisms (2,23,24). As we observed difficulties with expression and cloning of TOGARAM1, we switched to using its mouse homolog crescerin (from now on referred to as mCrescerin1). mCrescerin1 and TOGARAM1 have the same domain structure and share over 85% sequence similarity (5). Purified TOG2 and TOG4 of mCrescerin1 have been shown to possess microtubule polymerase activity (23). In vitro, full length mCrescerin1 acts as a rescue factor, causing depolymerizing microtubules to convert back to growth, and slightly reduces overall microtubule growth rate (5).

Spindle pole associated protein 1, CSPP1, is viewed as a core centrosomal component. It localizes to spindle poles and the central spindle during mitoses and to centrosomes, centriolar satellites and ciliary axonemes during interphase (15,25,26). It comes in both a long and short isoform (CSPP1-S and CSPP1-L). CSPP1-L is the predominantly expressed isoform, although relative expression levels for both isoforms fluctuate asynchronously during the cell cycle (6,15,26). CSPP1 contributes to ciliogenesis and loss impacts cilia length and signalling capabilities (15). In vitro, CSPP1 localizes to damaged sites of the microtubule lattice and to the growing microtubule end, where it induces pauses followed by resumed growth, therefore displaying similar behaviour to microtubule stabilizing compounds such as taxanes (5,6,27). It has been determined with cryo-ET and minflux that CSPP1 binds to the microtubule lumen (6).

CCDC66 can be found in distinct cellular pools at centrioles, centriolar satellites and in primary cilia, divided over the basal body, ciliary axoneme and accumulated at the tip (16,28). CCDC66 plays a role in ciliogenesis and depletion leads to shorter cilia (16). In vitro, CCDC66 localizes to the microtubule lattice but does not affect overall microtubule dynamics, and is therefore viewed as a scaffold (5). Next to EB3, recruitment of CEP104 to the growing microtubule lattice can also be potentiated by CCDC66. In this instance, lattice blocks are observed in which the microtubule very slowly depolymerizes (5).

ARMC9 does not have any functional domains known to directly interact with microtubules and therefore like CCDC66 is viewed as a scaffold within the tip module (2,5). In vitro, ARMC9 gets recruited to microtubules by CSPP1 and mCrescerin1 but not by CEP104 or CCDC66. Yet the role of this recruitment to overall microtubule dynamics regulation is not clear (5). Previous studies have reported direct interactions through GAL-2 based yeast two hybrid (Y2H) screens for ARMC9 with CSPP1, CCDC66 and TOGARAM1 (2). In cells ARMC9 localizes to centrioles, basal bodies and primary cilia, but redistributes to accumulate at the ciliary tip upon stimulation of Hedgehog signalling (7,14,29). Combined with the observation that loss of ARMC9 results in lower levels of ciliary accumulation of GLIs, important targets of Hedgehog, ARMC9 is viewed as a ciliary signalling factor and suspected to be involved in trafficking and/or retention of other signalling molecules at the ciliary tip (14,30). In motile cilia, ARMC9 has been shown to localize to axonemal B-tubules together with mCrescerin1, where they have an opposite function in regulating length (24). It is not known if this also holds for primary cilia.

Unpublished date from our lab show that all five tip module proteins combined in vitro lead to very slowly but steadily growing microtubules that do not undergo catastrophes, a phenomenon that was termed slow growth (5). Slow growth demonstrates a novel kind of microtubule regulation in which a single group of proteins can both stabilize GDP-lattices to prevent microtubule shrinking as well as facilitate new GTP tubulin addition, and therefore allow microtubule growth independent of a GTP-cap (5). Although unpublished cryo-ET data from our lab recently confirmed that the tip module indeed forms one big complex at a microtubule tip, the exact geometry of individual proteins within this complex remains unclear. Determining how tip module proteins interact and form the overall complex could contribute to obtaining a better understanding of how slow growth is facilitated. In this study, we therefore extended the interaction map of the ciliary tip module by narrowing down various interactions to specific functional domains or protein regions, and highlighted their biological relevance by showing that Joubert syndrome patient mutations can disrupt these interactions.

Results

Ciliary tip module proteins interact with each other, localize to primary cilia, and all except ARMC9 co-localize with cytoplasmic microtubules upon overexpression

The five proteins comprising the ciliary tip module have a varied domain organization (fig 1A) (5). Previous studies showed that ARMC9 directly interacts with CSPP1, TOGARAM1 and CCDC66 (2). In order to corroborate these findings, we carried out a co-immunoprecipitation (co-IP) assay with all tip module proteins with an mCherry tag against GFP tagged ARMC9 (fig 1B). We note that by working with overexpressed proteins from cell lysate, we cannot prove interactions to be direct. All tip module proteins except for CEP104 and CSPP1 co-precipitated with ARMC9. mCherry tagged CSPP1 (long isoform) showed high levels of cytoplasmic aggregation when overexpressed in HEK293T cells, which we suspected to affect its ability to interact with ARMC9. Indeed, a reciprocal co-IP assay with GFP tagged CSPP1 and mCherry tagged ARMC9 showed strong co-precipitation (fig 1C).

All tip module proteins have been shown to localize to primary cilia and all but ARMC9 to localize to microtubules upon overexpression (2,5,16,18,29,31). To confirm these findings, we overexpressed GFP tagged full length tip module proteins in inner medullary collecting duct 3 (IMCD3) cells and stained for acetylated and tyrosinated tubulin to visualize primary cilia and cytoplasmic microtubules, respectively (fig 1D,E). IMCD3 is a murine derived cell line able to form primary cilia in culture without any stimulation like serum starvation and is one of the most commonly used cell lines to study primary cilia (32). All tip module proteins localized to primary cilia and all but ARMC9 showed localization to cytoplasmic microtubules. CCDC66 and mCrescerin1 caused some microtubule bundling at higher expression levels (fig 1D). Interestingly, we also observed localization to cytoplasmic bridges either at overexpression or with immunostaining for mCrescerin1 and ARMC9 and confirmed previously observed localization for CSPP1 and CCDC66 (33,34) (fig S1A,B).

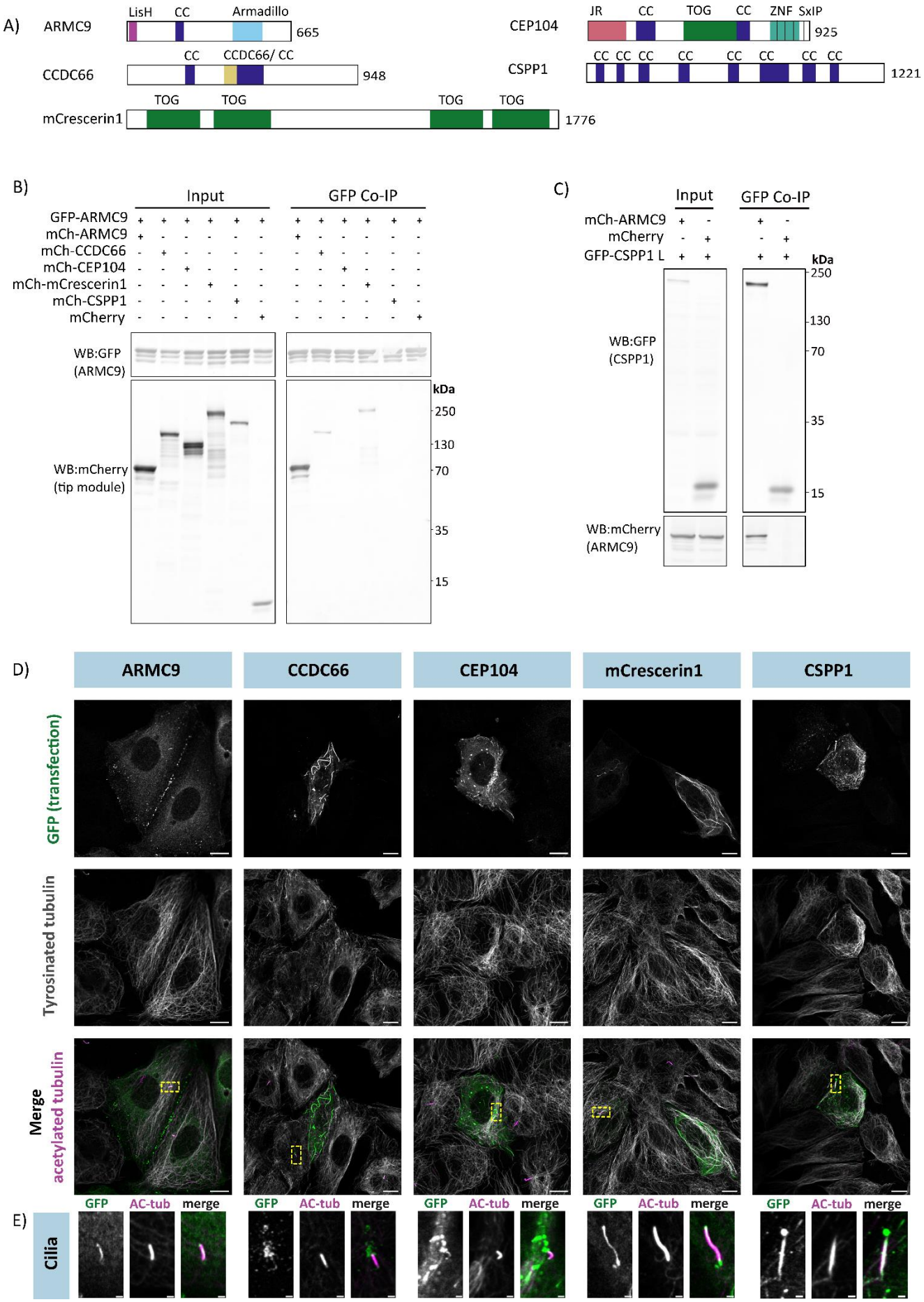
A)
ARMC9
LisH
CC
Armadillo
665
CCDC66
CC
CCDC66/ CC
948
mCrescerin1
TOG
TOG
TOG
TOG
1776
CEP104
JR
CC
TOG
CC
ZNF
SxIP
925
CSPP1
CC CC CC
CC
CC
CC
CC CC
1221
B)
Input
GFP Co-IP
GFP-ARMC9
mCh-ARMC9
mCh-CCDC66
mCh-CEP104
mCh-mCrescerin1
mCh-CSPP1
mCherry
WB:GFP
(ARMC9)
WB:mCherry
(tip module)
kDa
250
130
70
35
15
C)
Input
GFP Co-IP
mCh-ARMC9
mCherry
GFP-CSPP1 L
kDa
250
130
70
35
15
WB:GFP
(CSPP1)
WB:mCherry
(ARMC9)
D)
ARMC9
CCDC66
CEP104
mCrescerin1
CSPP1
GFP (transfection)
Tyrosinated tubulin
Merge
acetylated tubulin
E)
Cilia
GFP
AC-tub
merge

Figure 1. Ciliary tip module proteins; interaction and cellular localization upon overexpression *(A) Schematic representation of all full length ciliary tip module proteins. LisH; lissencephaly type 1-like homology motif, CC; coiled-coil domain, ARM; armadillo repeats, JR; jelly roll, TOG; tumor overexpressed gene domain, ZNF; zinc finger arrays (B) GFP co-IP of GFP tagged full length ARMC9 with mCherry tagged full length: ARMC9, CCDC66, CEP104 and mCrescerin1. Western blot (WB) analysis after GFP targeted immunoprecipitation indicated the presence of mCherry tagged ARMC9, CCDC66 and mCrescerin1, confirming interactions. GFP-tagged ARMC9 showed no interaction with mCherry tagged CEP104, CSPP1 and mCherry. mCherry served as a negative control. (C) GFP co-IP of GFP tagged full length CSPP1 (long isoform) or GFP with mCherry tagged full length ARMC9. WB analysis after GFP targeted immunoprecipitation indicated the presence of mCherry tagged ARMC9, confirming interaction. mCherry tagged ARMC9 showed no interaction with GFP, which served as a negative control. (D) Zeiss Lsm700 63x confocal fluorescence images of fixed murine inner medullary collecting duct (IMCD3) cells overexpressing GFP- tagged full length: ARMC9, CEP104, CCDC66, mCrescerin1 and CSPP1 (long isoform). Primary cilia and microtubules are visualized by immunostaining for acetylated tubulin and tyrosinated α-tubulin, respectively. Scale bar, 10 µm. (E) close-ups of images displayed in 1D, showing primary cilia. Scale bar, 1 µm.*

ARMC9 and mCrescerin1 co-localize to cytoplasmic microtubules upon overexpression

In various experimental settings both in vivo and in vitro, ARMC9 and TOGARAM1 have been shown to interact (2,5). To confirm these findings, we overexpressed mCherry tagged mCrescerin1 and GFP tagged ARMC9 both separately and together in COS7 cells and stained for acetylated and tyrosinated tubulin (fig 2A). It has previously been observed that overexpressed mCrescerin1 localizes along the lattice of cytoplasmic microtubules and causes bundling (23). Although cytoplasmic co-localization with microtubules is unlikely to be biologically relevant, as it is only observed upon overexpression and not when staining for the endogenous protein (fig S1A), it can be used as an assay to probe interaction with microtubules or other proteins (23). In line with previous observations (fig 1C) (5,23), overexpressed ARMC9 remained diffuse in the cytoplasm but mCrescerin1 localized to cytoplasmic microtubules and caused bundling (fig 2A). Signal of acetylated tubulin, a post translational modification common to axonemal microtubules in primary cilia (23), appeared to increase when microtubules were decorated by mCrescerin1 in transfected cells, but this was not quantified. Upon co-transfection, ARMC9 got strongly recruited by mCrescerin1, confirming the interaction and indicating that microtubule binding by mCrescerin1 is quite robust as presence of ARMC9 does not cause mCrescerin1 to dissociate from microtubules (fig 2A). The recruitment of ARMC9 to cytoplasmic microtubules by mCrescerin1 appears to be quite strong, as cytoplasmic signal of ARMC9 was either completely lost or highly reduced, depending on mCrescerin1 expression levels (fig 2A). Moreover, co-localization between microtubules and mCrescerin1 resulted in increased bundling and the cytoplasmic background signal, as observed for single mCrescerin1 transfections, was either lost or highly reduced (fig 2A). These observations suggest that ARMC9 can enhance the ability of mCrescerin1 to localize to cytoplasmic microtubules. Altogether, these results indicate that overexpressed mCrescerin1 co-localizes with cytoplasmic microtubules and can recruit ARMC9, which in turn enhances mCrescerin1's own localization.

ARMC9 is a dimer in solution but can interact with mCrescerin1 through its armadillo repeat in a monomeric state

Direct interaction between TOGARAM1 and ARMC9 have previously been mapped to be dependent on a C-terminal fragment of ARMC9 containing a coiled-coil (CC) and an armadillo repeat (ARM) domain by Y2H screens (2). We set out to narrow down the site of ARMC9 that facilitates interaction with mCrescerin1 to a single functional domain or smaller protein region. As CC domains are known to facilitate protein multimerization (19,35) and co-IP of full length ARMC9 with itself demonstrates a propensity for multimerization (fig 1B), it raised the question of whether ARMC9 might need to multimerize in order to interact with mCrescerin1. We first determined the multimeric state of ARMC9 in solution using single

molecule counting. By comparing intensities of GFP and GFP tagged EB3, a known monomer and dimer respectively, to the intensity of GFP tagged ARMC9, we found that ARMC9 is a dimer in solution (fig 2B). To assess if the CC domain of ARMC9 is essential for dimerization, we repeated the assay with an ARMC9 construct missing its CC domain (ARMC9 ΔCC) (fig 2C). Intensity now was close to the intensity of single GFP, indicating the CC domain is necessary for dimerization.

To narrow down the site of ARMC9 important for interaction with mCrescerin1, we performed a co-IP assay with mCrescerin1 and various ARMC9 domain truncations (fig 2 D,E). Only ARMC9 constructs containing the ARM domain co-precipitated with mCrescerin1, including ARMC9 ΔCC, indicating that indirect interaction between mCrescerin1 and ARMC9 in co-IP is solely dependent on the ARM domain and independent of the multimeric state of ARMC9 (Fig 2 D,E). To further evaluate the dependency on the ARM domain for interaction between ARMC9 and mCrescerin1, we transiently transfected COS7 cells with the ARMC9 domain truncation constructs (fig 2E) together with full length mCrescerin1 and stained for tyrosinated and acetylated tubulin (fig S2A). ARMC9 ΔLisH and ΔCC showed similar results to full length ARMC9 and co-localized with mCrescerin1 to cytoplasmic microtubules, which is in agreement with our co-IP (fig 2D). ARMC9 ΔARM showed cytoplasmic aggregation and, to our surprise, could still co-localize to microtubules upon co-transfection with mCrescerin1 (fig S2A). Although co-localization to microtubules for both proteins appeared to be slightly less pronounced, interaction was nonetheless still observed, contradicting the result of the aforementioned co-IP. Altogether, results indicate that the ARM domain of ARMC9 facilitates interaction with mCrescerin1 and that even though ARMC9 is a dimer in solution, it can interact with mCrescerin1 independent of its dimeric state.

The tubulin binding surface of mCrescerin1 TOG2 facilitates interaction with ARMC9

We next sought to determine the region of mCrescerin1 that is important for interaction with ARMC9. Direct interaction between TOGARAM1 and ARMC9 has previously been mapped to the N-terminal region containing the first two TOG domains(2) and with a co-IP assay we confirmed this also holds true for its mouse homologue, mCrescerin1 (fig S2B,C). To narrow down the interaction site to one TOG domain specifically, we performed a co-IP assay with ARMC9 and various mCrescerin1 constructs containing point mutations in the intra-HEAT loops of TOG1 and TOG2 (Fig 2E,F). TOG domains are built up from six α-helix pairs termed HEAT repeats that are linked together by intra-HEAT loops, which form a solvent-exposed plane in the tertiary protein structure which has previously been characterized to directly bind to tubulin (23,36). The selected mutations disrupt the predicted tubulin binding surface without disrupting the overall TOG domain fold (23). Co-IP results indicate that TOG2 is the binding site of ARMC9 (Fig 2E,F). Interestingly, this suggests that mCrescerin1 can utilize what has previously been categorized as a tubulin binding surface (23) for interaction with other proteins as well.

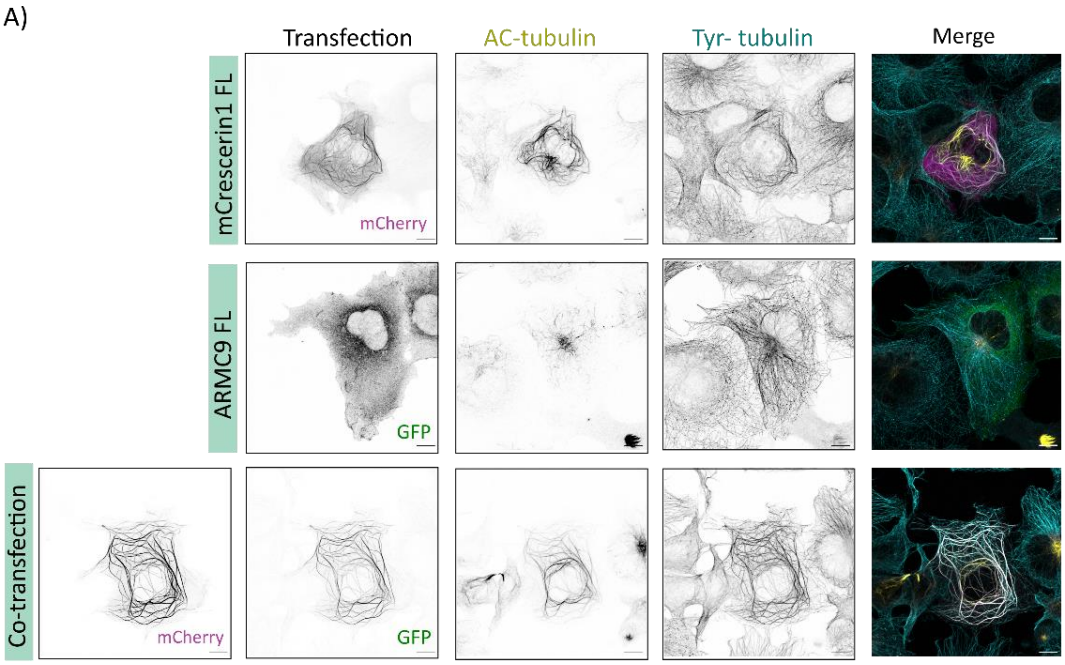
A)
Transfection
AC-tubulin
Tyr- tubulin
Merge
mCrescerin1 FL
ARMC9 FL
Co-transfection
mCherry
GFP

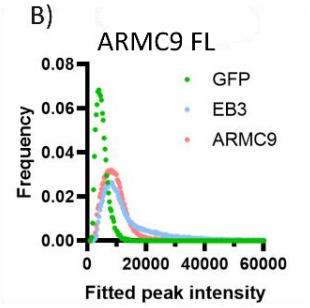
B)
ARMC9 FL
GFP
EB3
ARMC9
Frequency
Fitted peak intensity

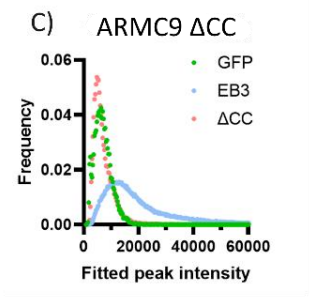
C)
ARMC9 ΔCC
GFP
EB3
ΔCC
Frequency
Fitted peak intensity

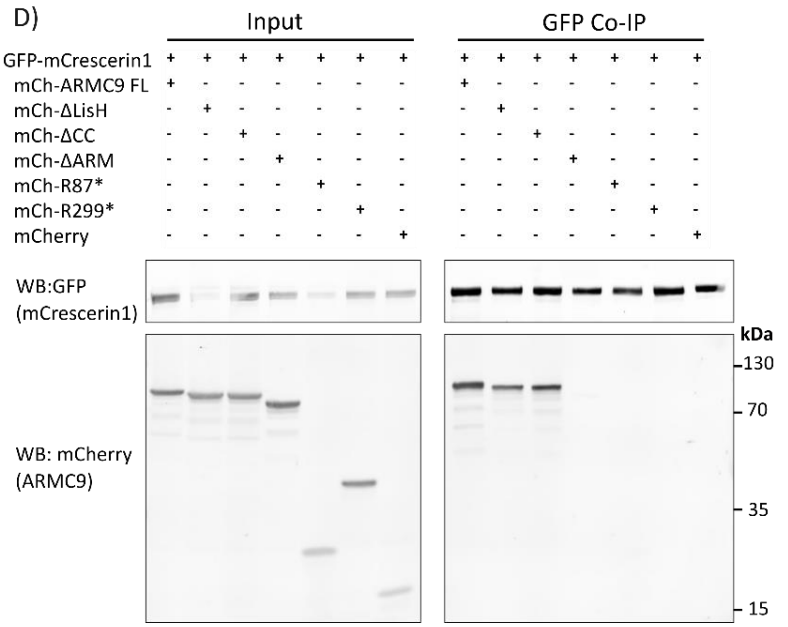
D)
Input
GFP Co-IP
GFP-mCrescerin1
mCh-ARMC9 FL
mCh-ΔLisH
mCh-ΔCC
mCh-ΔARM
mCh-R87*
mCh-R299*
mCherry
WB:GFP
(mCrescerin1)
WB: mCherry
(ARMC9)
kDa
130
70
35
15

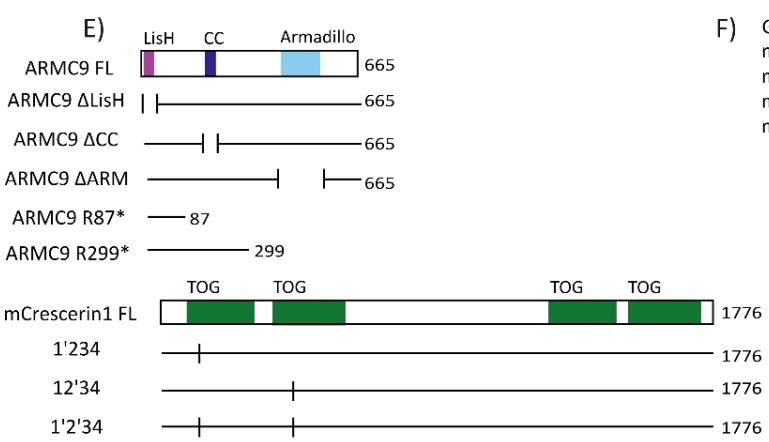
E)
LisH
CC
Armadillo
ARMC9 FL
ARMC9 ΔLisH
ARMC9 ΔCC
ARMC9 ΔARM
ARMC9 R87*
ARMC9 R299*
665
87
299
TOG
mCrescerin1 FL
1'234
12'34
1'2'34
1776

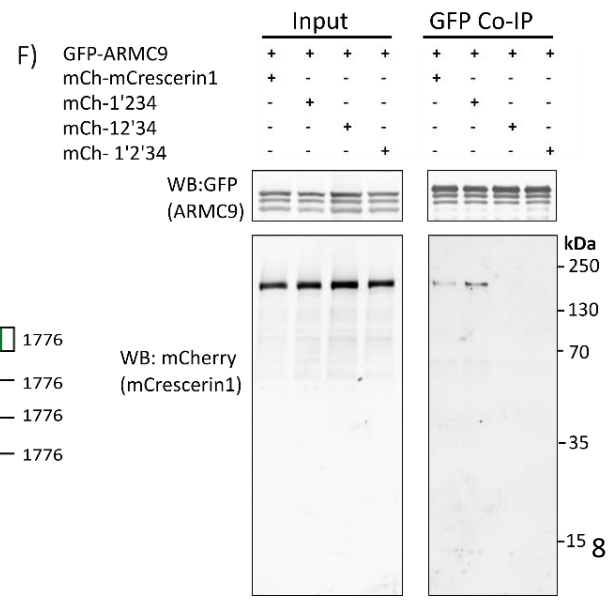
F)
Input
GFP Co-IP
GFP-ARMC9
mCh-mCrescerin1
mCh-1'234
mCh-12'34
mCh- 1'2'34
WB:GFP
(ARMC9)
WB: mCherry
(mCrescerin1)
kDa
250
130
70
35
15

Figure 2. ARMC9 and mCrescerin1 interact through the armadillo repeat and TOG2 *(A) Zeiss Lsm700 63x confocal fluorescence images of fixed COS7 cells overexpressing GFP tagged full length ARMC9 , mCherry-tagged full length mCrescerin1 or both. Microtubules are visualized by immunostaining for acetylated tubulin and tyrosinated α-tubulin. Scale bar, 10 µm. (B-C) histograms of fluorescence intensities of GFP, GFP-EB3 and GFP-ARMC9 FL (B) or GFP-ARMC9 ΔCC (C) molecules in solution in separate chambers on a single slide. Number of molecules in analysis: GFP, N=18415/ 14914; GFP-EB3, N= 132826/163959 ; GFP-ARMC9, N= 99873 ; GFP-ARMC9ΔCC, N=55479. (D) GFP co-IP of GFP tagged full length mCrescerin1 with mCherry tagged ARMC9 constructs: full length, ΔlisH, ΔCC, ΔARM, R87* and R299*. mCherry was included as a negative control. WB analysis after GFP targeted immunoprecipitation indicated the presence of mCherry tagged ARMC9 FL, ΔlisH, and ΔCC but the absence of ΔARM, Q87*, R299* and mCherry. (E) Protein schematic of used constructs. 1234 correspond to the four TOG domains of mCrescerin1. 1'234; P109E, 12'34; Y364E. (F) GFP co-IP of GFP tagged full length ARMC9 with mCherry tagged mCrescerin1 constructs: full length, 1'234, 12'34 and 1'2'34. WB analysis after GFP targeted immunoprecipitation indicated the presence of mCherry tagged mCres FL and 1'234 but the absence of 12'34 and 1'2'34.*

JBTS mutations in the second TOG domain of mCrescerin1 disrupt ARMC9 binding

Dysfunction of the ciliary tip module is linked to the ciliopathy Joubert syndrome (JBTS) (2). Mutations in TOGARAM1, CEP104, ARMC9 and CSPP1, but not in CCDC66, have been reported in JBTS patients (table 1, table S1). Frameshifts and alternative splice events or similar variants likely result in mRNAs that are the target of nonsense mediated decay, as truncated proteins are seldom detected in cells (37,38). Therefore, these mutations often indirectly result in loss of protein(37). Point mutations leading to amino acid substitutions can however potentially alter protein functioning or structure, leading to disease, which is why we focussed on that type of JBTS variants in this study (39). A big fraction of JBTS associated mutations reported in TOGARAM1 are located within a short stretch of amino acids within the second α-helix of the first HEAT repeat of TOG2 (2,23) (fig 3A). We demonstrated TOG2 to be important for interaction between mCrescerin1 and ARMC9 using co-IP and it has previously been shown that interaction between ARMC9 and TOGARAM1 is completely disrupted by JBTS variants L373P and R368W, both through co-IP and Y2H screens (fig 2F) (2). To determine if the interaction with ARMC9 is also disrupted for the other two reported TOG2 JBTS variants, we modelled these mutations in mCrescerin1 by generating the mutants A371D, Q360* and L373P, of which the last one served as a negative control. In a co-IP assay, all TOG2 mutants completely abolished interaction with ARMC9 (fig 3B,D). These results add to previous findings suggesting that disrupted ARMC9 – TOGARAM1 interaction is related to Joubert syndrome and highlights the biological importance of this protein-protein interaction.

JBTS mutations in the armadillo repeat of ARMC9 do not necessarily effect mCrescerin1 binding

Unlike for TOGARAM1, reported JBTS variants in ARMC9 are evenly distributed over the length of the protein sequence and show no specific sites of accumulation (fig 3A). We showed the ARM domain of ARMC9 to be important for interaction with mCrescerin1 (fig 2D) and that JBTS point mutations in TOG2, the indicated interaction site of mCrescerin1, completely disrupts ARMC9-mCrescerin1 Interaction (fig 3B,D). Therefore, we next sought to determine if JBTS associated mutations in the ARM domain would also disrupt ARMC9 – mCrescerin1 interaction. We generated constructs for the point mutants G492R, P520L and R445C, located in or just before the ARM domain, and implemented them in a co-IP assay against full length mCrescerin1 (fig 3C). Only mutant G492R showed reduced co-precipitation in comparison to WT ARMC9 (fig 3C,E). Overall, these results indicate that reported JBTS mutations in ARMC9 in or close to the ARM domain do not necessarily affect ARMC9 – mCrescerin1 interaction, suggesting they are pathogenic in a different way.

Table 1. *Gene variants in individuals with ARMC9, TOGARAM1 or CEP104 related JBTS. Domain annotation in accordance to annotation used source reporting the variant* (2,29,40–42)*.*

Mutation	Functional domain	Pt. Identifier	source
ARMC9			
205G>A (G68R)	NA	UW132-3 (and -4)	*(Van de Weghe et al., 2017)* (29) *(Latour et al.,2020)* (2)
1336C>T (R446C)	NA	UW132-3 (and -4)	*(Van de Weghe et al., 2017)*(29) *(Latour et al., 2020)* (2)
259C>T (R87*)	NA	UW335-3 (and -4)	*(Van de Weghe et al., 2017)* (29)
1027C>A (R343S)	NA	UW335-3 (and -4)	*(Van de Weghe et al., 2017)*(29) *(Latour et al., 2020)* (2)
51+ 5G>T (splice)	NA	UW348-3	*(Van de Weghe et al., 2017)* (29)
1027C>T (R343C)	NA	UW349-3, UW116-3, LRO9-023, SA1-3	*(Van de Weghe et al., 2017)* (29) *(Wang et al., 2022)* (40)
1211 - 1334 del (R405A fs*7)	NA	UW116-3	*(Van de Weghe et al., 2017)*(29) *(Latour et al., 2020)* (2)
1474+1G>C (splice)	NA	UW349-3	*(Van de Weghe et al., 2017)* (29)
1474 G>A (G492R)	ARM	LR0-23	*(Van de Weghe et al., 2017)* (29)
1559 C>T (P520L)	ARM	SA2-3, SA2-4	*(Van de Weghe et al., 2017)* (29)
895 C>T (R299*)	NA	NA	*(Wang et al., 2022)* (40)
1878+1G > A (splice)	NA	NA	*(Wang et al., 2022)* (40)
mCrescerin1			
1124T>C (L373P)	TOG2	UW351-3	*(Latour et al., 2020)* (2)
3931 C>T (R1311C)	TOG3	UW351-3	*(Latour et al., 2020)* (2)
1084C>T (Q362*)	TOG2	UW360-3	*(Latour et al., 2020)* (2)
del14q21.2: g.45472062- 45484253 (12 kb deletion spanning exons 4-7)	NA	UW360-3	*(Latour et al., 2020)* (2)
1102C>T (R368W)	TOG2	13DG1578	*(Latour et al., 2020)* (2)
3248C>A (S1083*)	Central linker	WGL-1914	*(Latour et al., 2020)* (2)
1112C>A (A371D)	TOG2	JAS-L50	*(Latour et al., 2020)* (2)
5023C>T (R1675*)	TOG4	JAS-L50	*(Latour et al., 2020)* (2)
CEP104			
735+2T>C (intron retention)	CC 1	1763.618 (homozygous)	*(Srour et al., 2015)* (41)
2572-2A>G (effect unknown)	NA	GeneDx01	*(Srour et al., 2015)* (41)
496C>T (R166*)	NA	GeneDx01	*(Srour et al., 2015)* (41)
1328-1329 insT (Y444fs*3)	TOG	842629 (homozygous)	*(Srour et al., 2015)* (41)
2364 +1G>A (506nt intron retention, resulting in early termination)	NA	102C	*(Luo et al., 2019)* (42)
414delC (Asn138Lys fs*11)	JR	102C	*(Luo et al., 2019)* (42)
(331C>T) R111W	JR	NA	*Roepman lab, unpublished*

JBTS point mutant R1313C in mCrescerin1 impairs its ability to localize to cytoplasmic microtubules upon overexpression

A single JBTS associated TOGARAM1 variant has been reported in TOG3, point mutation R1311C. (table 1, Fig 3A). As TOG3 has previously been implicated to contribute to the ability of mCrescerin1 to bind to microtubules (23), we set out to determine if the R1311C variant would disrupt this interaction. We modelled the JBTS variant as R1313C in mCrescerin1, transiently transfected COS7 cells and stained for tyrosinated α-tubulin (fig 3F,G). Compared to WT mCrescerin1, the R1313C variant showed much less interaction with cytoplasmic microtubules (fig 3F,G). Interestingly, by co-transfecting with ARMC9, the R1313C variant could strongly localize to microtubules again, at levels appearing to be similar to the wild type (fig 3G). In conclusion, TOG3 JBTS variant R1313C appears to affect the localization of mCrescerin1 to cytoplasmic microtubules, but this reduced localization is no longer observed upon co-transfection with ARMC9.

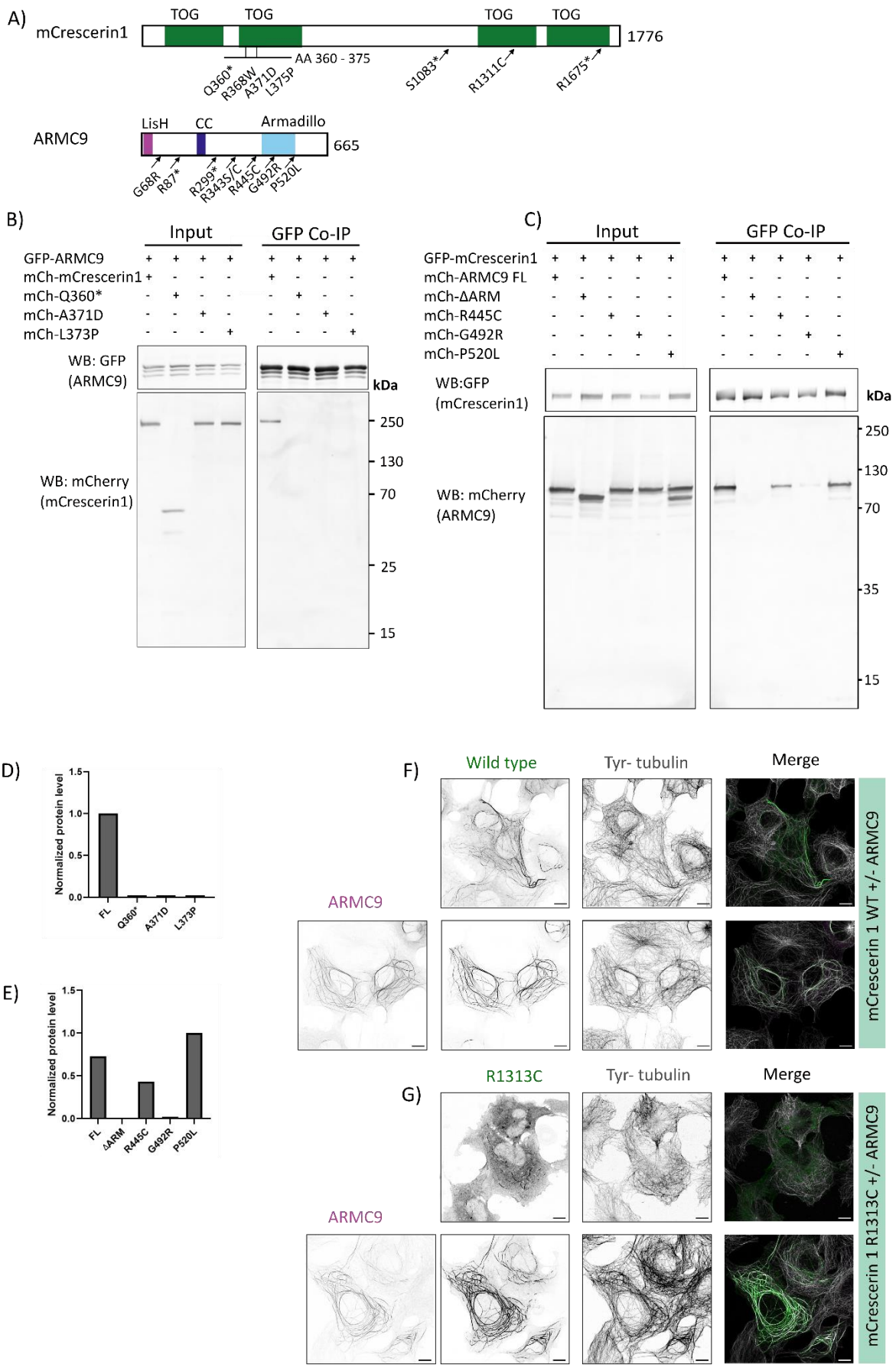
A)
mCrescerin1
TOG
TOG
TOG
TOG
1776
AA 360 - 375
Q360*
R368W
A371D
L375P
S1083*
R1311C
R1675*
ARMC9
LisH
CC
Armadillo
665
G68R
R87*
R299*
R343S/C
R445C
G492R
P520L
B)
Input
GFP Co-IP
GFP-ARMC9
mCh-mCrescerin1
mCh-Q360*
mCh-A371D
mCh-L373P
WB: GFP
(ARMC9)
WB: mCherry
(mCrescerin1)
kDa
250
130
70
25
15
C)
Input
GFP Co-IP
GFP-mCrescerin1
mCh-ARMC9 FL
mCh-ΔARM
mCh-R445C
mCh-G492R
mCh-P520L
WB:GFP
(mCrescerin1)
WB: mCherry
(ARMC9)
kDa
250
130
70
35
15
D)
Normalized protein level
1.5
1.0
0.5
0.0
FL
Q360*
A371D
L373P
E)
Normalized protein level
1.5
1.0
0.5
0.0
FL
ΔARM
R445C
G492R
P520L
F)
Wild type
Tyr- tubulin
Merge
ARMC9
mCrescerin 1 WT +/- ARMC9
G)
R1313C
Tyr- tubulin
Merge
ARMC9
mCrescerin 1 R1313C +/- ARMC9

Figure 3. mCrescerin1 JBTS associated mutations affect ARMC9-mCrescerin1 interaction *(A) Schematic of variants documented for individuals with ARMC9 and TOGARAM1 related JBTS. (B) GFP co-IP of GFP tagged full length ARMC9 with mCherry tagged mCrescerin1 constructs: full length, Q360*, A371D and L373. WB analysis after GFP targeted immunoprecipitation based purification indicated the presence of mCherry tagged mCrescerin1 FL but the absence of all aforementioned mCrescerin1 JBTS mutations. C) GFP co-IP of GFP tagged full length mCrescerin1 with mCherry tagged ARMC9 constructs: full length, ΔARM, R445C, G492R and P520L. WB analysis after GFP targeted immunoprecipitation based purification indicated the presence of mCherry tagged ARMC9 FL, R445C and P520L but the absence of ΔARM. G492R showed highly reduced co-precipitation in comparison to other constructs. (D) and (E) Quantification of western blots. All intensities were measured in FIJ. Signal of mCherry tagged construct was first normalized to GFP tagged construct and then co-IP signal was normalized to input signal. Data is normalized to 1. F) and G) Zeiss Lsm700 63x confocal fluorescence images of fixed COS7 cells overexpressing (F) GFP tagged mCrescerin1 full length or (G) mCrescerin1-R1313C co-transfected with mCherry tagged ARMC9. Microtubules are visualized by Immunostaining for tyrosinated α-tubulin. Scale bar, 10 µm.*

CSPP1 interacts through its C-terminal region with a linker region of ARMC9

We next sought to further characterize the involved protein regions in the interaction between ARMC9 and CSPP1. CSPP1 has many helical domains and comes in two splice isoforms (CSPP1-S and CSPP1-L), of which the short isoform lacks an N-terminal region and has a small 51 amino acid internal deletion (6). CSPP1 has previously been shown to bind to the microtubule lumen, and though it has not been determined for mCrescerin1 specifically, other TOG domain protein families like CLASPs and XMAP215 are known to locate to the lattice (6,43). As expected, we did not observe interaction between mCrescerin1 and CSPP1 (both -S and -L) in co-IP experiments (fig 4A), which raises the question of how these proteins are linked within the entire tip module complex. As ARMC9 has been shown to directly interact with both CSPP1 and TOGARAM1 (2), we identified ARMC9 as a possible candidate to scaffold indirect interaction and set out to study the interaction between ARMC9 and CSPP1 further. Through a co-IP assay with full length CSPP1-S and various ARMC9 constructs (fig 2F), we mapped the binding site on ARMC9 for CSPP1 to a linker region between amino acids 87 and 299 (fig 4B). As ARMC9 ΔCC still co-precipitated, the binding region excludes the CC domain. This also suggests that ARMC9 can interact with CSPP1 as a monomer, similar to what we previously observed for mCrescerin1 (fig 2E). A reciprocal co-IP assay with full length ARMC9 and various CSPP1 constructs showed the interaction to depend on a c-terminal region of CSPP1, which has previously been characterized as the centrosome targeting region (figure 4C,D). This region is identical in both CSPP1 isoforms (6). Altogether, we showed that ARMC9 interacts through a linker region with the centrosome targeting region of CSPP1 and could possibly act as a scaffold to facilitate indirect interaction between mCrescerin1 and CSPP1.

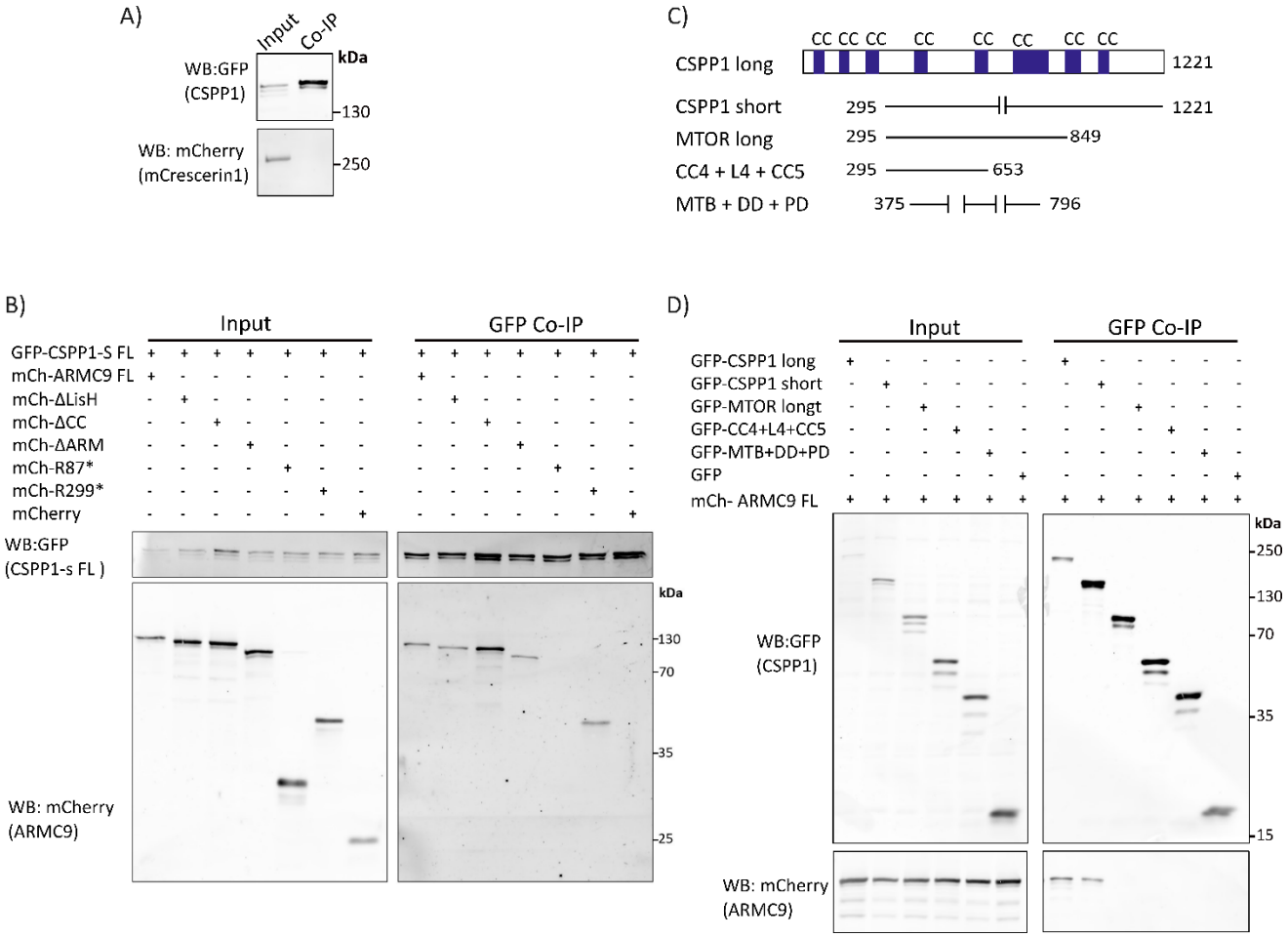

Figure 4. CSPP1 does not interact with mCrescerin1 but CSPP1 and ARMC9 interaction is facilitated by the centrosome targeting region of CSPP1 and a further undefined protein region of ARMC9 *(A) GFP co-IP of GFP tagged full length CSPP1-S and mCherry tagged full length mCrescerin1. WB analysis after GFP targeted immunoprecipitation indicated the absence of mCrescerin1. (B) GFP co-IP of GFP tagged full length CSPP1 (short isoform) with mCherry tagged ARMC9 constructs: full length, ΔlisH, ΔCC, ΔARM, R87* and R299*. mCherry was included as a negative control. WB analysis after GFP targeted immunoprecipitation indicated the presence of mCherry tagged ARMC9 FL, ΔlisH, and ΔCC, ΔARM and R299* but the absence of Q87* and mCherry. (C) Protein schematic displaying CSPP1 constructs implemented in co-IP. CC; coiled-coil, L; linker region, MTB; microtubule binding domain, DD; dimerization domain, PD; pausing domain. (D) GFP co-IP of GFP tagged CSPP1 constructs: long isoform, short isoform, microtubule organization centre long isoform (MTOR L), CC4 + L4 + CC5 and MTB + DD (CC5) + PD (CC6)* (6) *and mCherry tagged full length ARMC9. WB analysis after GFP targeted immunoprecipitation indicated the presence of mCherry- ARMC9 in the fractions containing CSPP1 FL long or short isoform and the absence in all other fractions. GFP was included as a negative control.*

Cytosolic localization of overexpressed CEP104 is affected by disrupting its SxIP motif and TOG domain

We then turned our attention to the tip module protein CEP104. CEP104 contains multiple functional domains, including a TOG domain and a SxIP motif (fig 1A). Direct interaction between CEP104, tubulin and EBs has previously been shown and CEP104 is known to localize to EB positive microtubule plus ends in cells and in vitro (5,19). To study how the different functional domains of CEP104 contribute to its cellular localization in regard to microtubules, we transiently transfected COS7 cells with GFP tagged CEP104 constructs individually missing specific functional domains (Fig 5A,B). Full length CEP104 showed co-localization with both EB1 and the growing ends of cytoplasmic microtubules. This localization pattern was similar for CEP104 ΔJR and ΔZNF (fig 5B). Disruption of the SxIP motif by mutation to SxNN resulted in complete loss of co-localization with EB1. Most of the CEP104 SxNN signal was diffusive in the cytoplasm, but

in cells with high expression levels some localization to the microtubule lattice could still be observed. Interestingly, CEP104 ΔTOG also lost co-localization with EB1. It still localized to microtubules, but completely lost plus end specificity and similar to SxNN was distributed evenly along the microtubule lattice (fig 5B). Taken together, these results suggest that the cytoplasmic localisation of CEP104 upon overexpression differently depends on interaction with EB1, the SxIP motif and the TOG domain.

CEP104 and mCrescerin1 interact through the zinc finger array and the central linker

Motivated by previous studies showing indirect interaction between CEP104 and TOGARAM1 through co-IP (2), we set out to determine which domains are important for this interaction. Through reciprocal co-IP assays, we confirmed interaction between mCrescerin1 and CEP104 and mapped interaction to be dependent on the central linker and the zinc finger region, respectively (fig 5A,C,D).

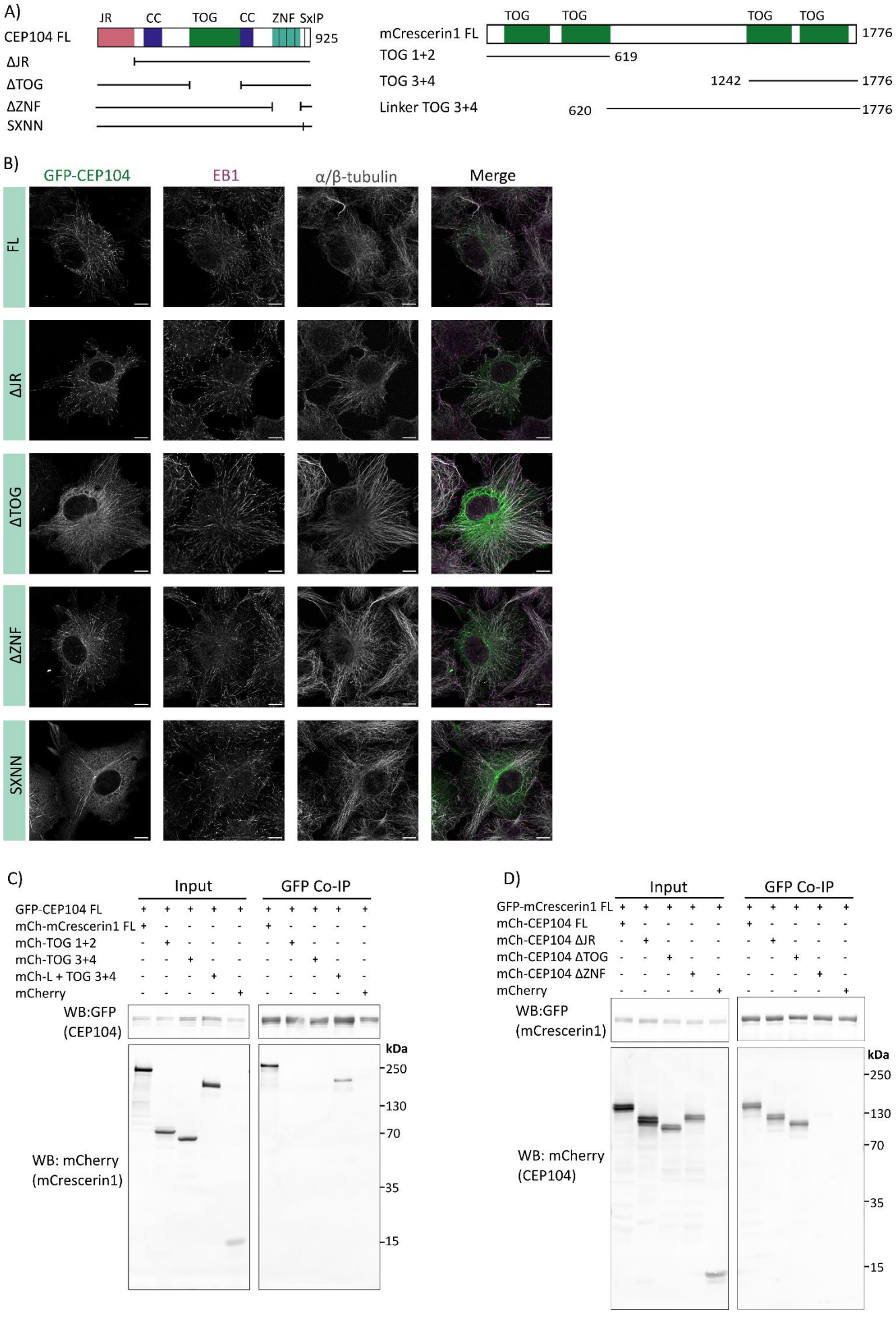
A)
JR
CC
TOG
CC
ZNF SxIP
CEP104 FL
925
ΔJR
ΔTOG
ΔZNF
SXNN
TOG
TOG
TOG
TOG
mCrescerin1 FL
1776
TOG 1+2
619
TOG 3+4
1242
1776
Linker TOG 3+4
620
1776
B)
GFP-CEP104
EB1
α/β-tubulin
Merge
FL
ΔJR
ΔTOG
ΔZNF
SXNN
C)
Input
GFP Co-IP
GFP-CEP104 FL
mCh-mCrescerin1 FL
mCh-TOG 1+2
mCh-TOG 3+4
mCh-L + TOG 3+4
mCherry
WB:GFP
(CEP104)
WB: mCherry
(mCrescerin1)
kDa
250
130
70
35
15
D)
Input
GFP Co-IP
GFP-mCrescerin1 FL
mCh-CEP104 FL
mCh-CEP104 ΔJR
mCh-CEP104 ΔTOG
mCh-CEP104 ΔZNF
mCherry
WB:GFP
(mCrescerin1)
WB: mCherry
(CEP104)
kDa
250
130
70
35
15

Figure 5. CEP104 cellular localization and interaction with mCrescerin1 (A) *protein schematic of various CEP104 and mCrescerin1 constructs, implemented in fluorescence cell images and/ or co-IPs. (B) Zeiss Lsm700 63x confocal fluorescence images of fixed COS7 cells overexpressing GFP tagged CEP104: full length, ΔJR, ΔTOG, ΔZNF and SXNN. Immunostaining for EB1 and α/β-tubulin. Scale bar, 10 µm. (C) GFP co-IP of GFP tagged full length CEP104 with mCherry tagged CEP104 constructs: full length, TOG 1+2, TOG 3+4 and linker + TOG 3+4. WB analysis after GFP targeted immunoprecipitation indicated the presence of mCherry tagged mCrescerin1 FL and linker + TOG 3+4 but the absence of TOG 1+2 and TOG 3+4 and mCherry. mCherry was included as a negative control. (D) GFP co-IP of GFP tagged full length mCrescerin1 with mCherry tagged CEP104 constructs: full length, ΔJR, ΔTOG and ΔZNF. WB analysis after GFP targeted immunoprecipitation indicated the presence of mCherry tagged CEP104 FL, ΔJR and ΔTOG severely reduced co-precipitation with CEP104 ΔZNF. mCherry was included as a negative control.*

CEP104 JBTS patient mutation R111W affects interaction with CCDC66 and CSPP1

Recently, a point mutation in the jelly roll domain of CEP104 was detected in a genetic screen of a patient with JBTS (fig 6A). As interaction of CEP104 with CCDC66 and CSPP1 has previously been shown to depend on the JR domain (15,16,20), we set out to determine if the R111W mutant would disrupt these interactions. We performed Co-IP assays with either full length CCDC66 or CSPP1-S and CEP104 R111W with CEP104 ΔJR included as a negative control (fig 6 B-E). In line with previous findings, we observed no co-precipitation between CEP104 ΔJR and full length CSPP1-S or CCDC66 (15,16,20) (fig 6 B-E). In both cases, level of co-precipitation with the R111W mutant was highly reduced in comparison to WT CEP104 (fig 6 B-E). Interaction between mCrescerin1 and CEP104 was unaffected by the R111W variant (fig S3B), which is in line with our previous finding that the ZNF domain of CEP104 is important for this interaction (fig 5C). In conclusion, the CEP104 R111W JBTS variant disrupts the interaction of CEP104 with CSPP1-S and CCDC66, suggesting a possible mode of pathogenicity of the variant.

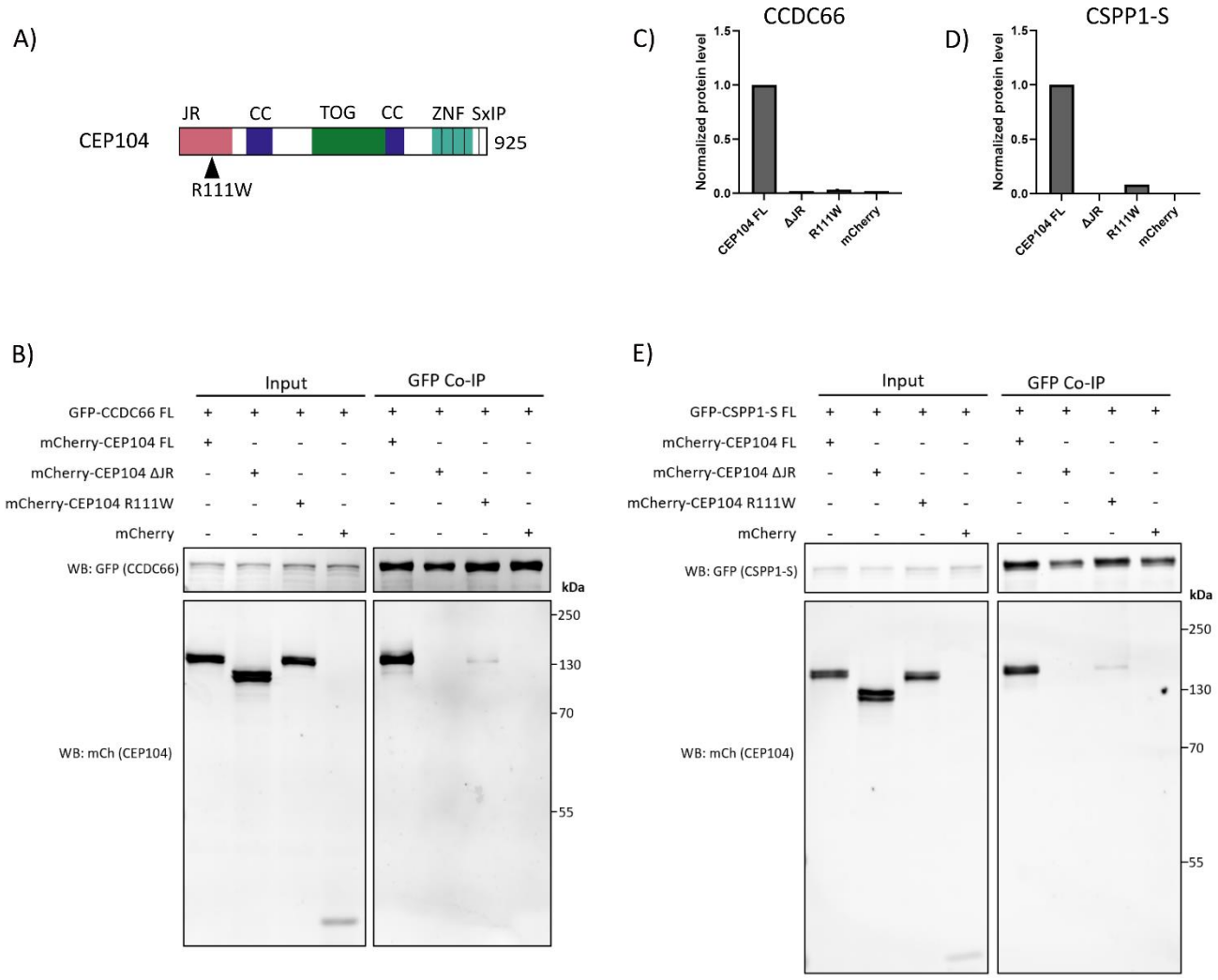

Figure 6. CEP104 JBTS variant R111W affects interaction between CEP104 and CCDC66 and CSPP1-S *(A) protein schematic displaying location of R111W mutation in CEP104 (B) GFP co-IP of GFP tagged full length CCDC66 with mCherry tagged CEP104 constructs: full length, ΔJR and R111W. WB analysis after GFP targeted immunoprecipitation indicated the presence of mCherry tagged CEP104 FL but the absence of ΔJR. Co-precipitation for R111W was highly reduced. mCherry was included as a negative control. (C-D) Quantification of WBs. All intensities were measured in FIJI signal of mCherry tagged constructs was first normalized to GFP tagged construct and then co-IP signal was normalized to input signal. Data is normalized to 1.(E) GFP co-IP of GFP tagged full length CSPP1-s with mCherry tagged CEP104 constructs: full length, ΔJR and R111W. WB analysis after GFP targeted immunoprecipitation indicated the presence of mCherry tagged CEP104 FL but the absence of ΔJR. Co-precipitation for R111W was highly reduced. mCherry was included as a negative control.*

A)

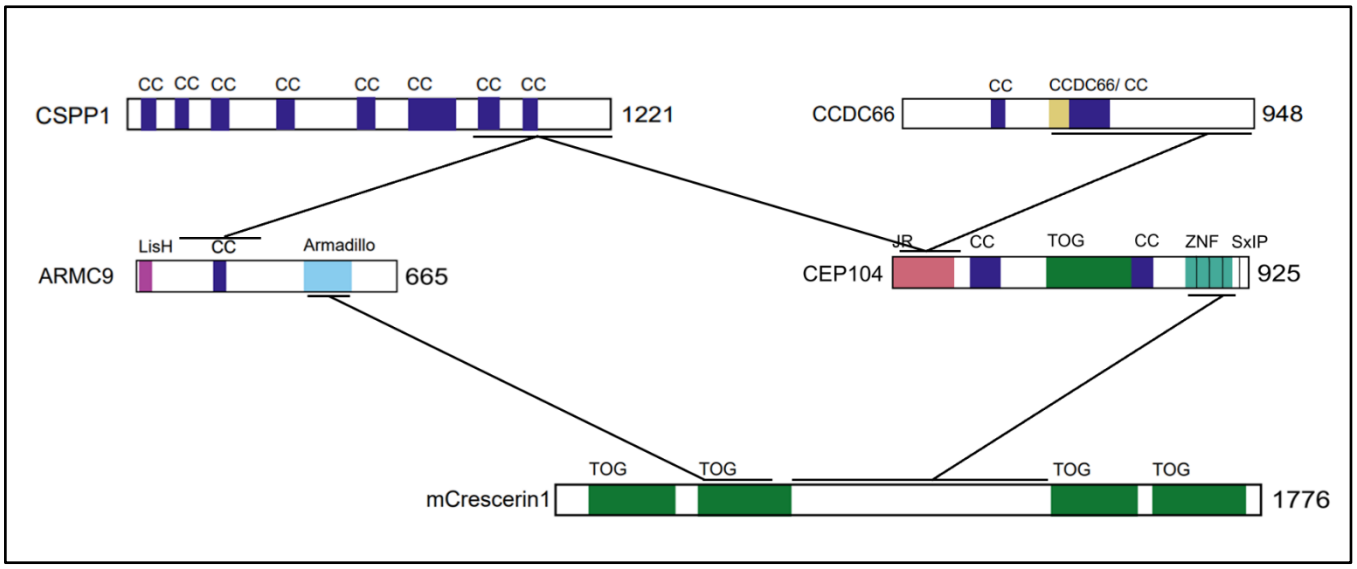

B)

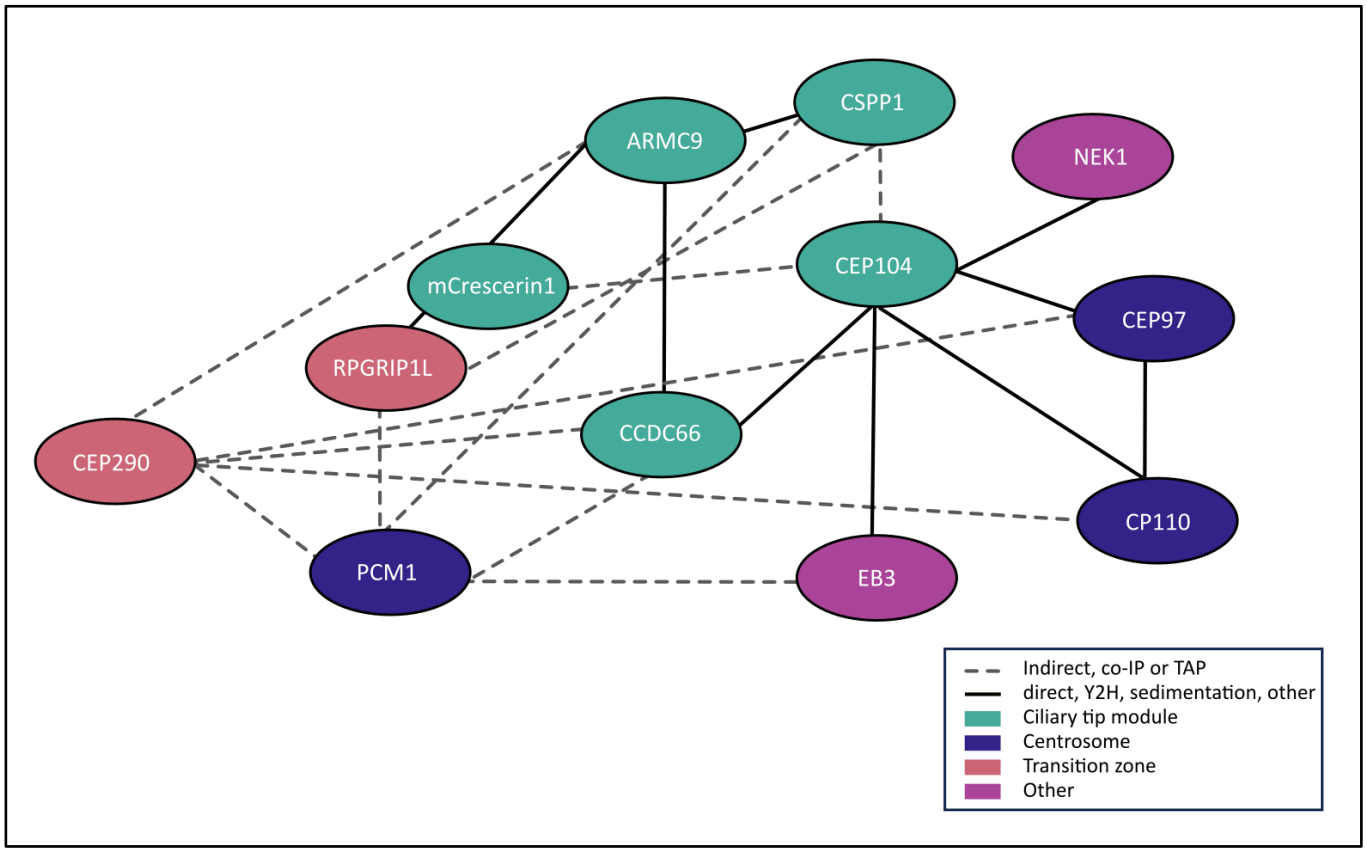

Figure 7. Ciliary tip module interaction maps *(A) Schematic overview of interactions within the ciliary tip module, either mapped or confirmed in this study. (B) (incomplete) extended ciliary tip module interaction map, placing tip module proteins in regulatory networks at centrioles/ centriolar satellites and at the ciliary transition zone. TAP; tandem affinity purification followed by mass spectrometry, Y2H; GAL-2 based yeast two hybrid screen.* (2,16,18,19,28,44–48)

Discussion

Ciliopathies, like Joubert syndrome (JBTS), encompass a collection of disorders marked by malfunctioning cilia. As ciliopathy patient-derived cells typically have cilia of abnormal lengths, it is suggested that cilia length and therefore axonemal microtubule regulation is crucial for proper functioning (2,4). Here, we further mapped protein-protein interactions between the core members of the ciliary tip module; a group of proteins suggested to regulate axonemal microtubule dynamics. Recent unpublished cryo-ET data from our lab demonstrated that tip module proteins form a single complex at microtubule ends. The exact geometry of individual proteins within this complex and how interactions are facilitated, especially when proteins are localized on opposite sides of the microtubule wall, however remains unclear. By performing multiple co-immunoprecipitations (co-IP) assays, we mapped interactions between (I)ARMC9 and mCrescerin1, (II) ARMC9 and CSPP1 and (III) CEP104 and mCrescerin1 to specific functional domains or protein regions, and confirmed from literature that the interaction of CEP104 with CCDC66 or CSPP1 is dependent on CEP104s jelly roll (JR) domain (fig 7A). Additionally, we showed that JBTS associated variants affect ARMC9-mCrescerin1, CEP104-CCDC66 and CEP104-CSPP1S interactions, highlighting the biological relevance of protein-protein interactions within the tip module.

We observed that overexpressed mCrescerin1 localized to cytoplasmic microtubules and caused bundling (fig 2A). This suggests an inherent ability of mCrescerin1 to interact with microtubules, in line with previous findings (23). TOGARAM1 (the human isoform of mCrescerin1) or ARMC9 depletion or dysfunction in either NIH-3T3 cells, JBTS patient fibroblasts, or in zebrafish have been linked to reduced acetylation and/or polyglutamylation, which are posttranslational modifications common to axonemal microtubules (2,7,8,14,23). Microtubule bundling requires some microtubule flexibility and is known to promote stability, linking bundling to acetylation (49). The observed co-localization of acetylated tubulin and mCrescerin1 and increased signal for acetylated tubulin in transfected COS7 cells, might suggest a potential role for mCrescerin1 in microtubule stabilization or in regulation of post-translational tubulin modifications. However, localization of mCrescerin1 to cytoplasmic microtubules was found to be an overexpression artifact, and we cannot exclude that mCrescerin1 ability to bundle microtubules represents an overexpression artefact as well (23). Therefore, further investigations are needed to determine the role of mCrescerin1 in microtubule stabilization or acetylation in primary cilia.

ARMC9 knockout in tetrahymena results in the most severe phenotypes compared to knockout of CHE-12 (mCrescerin1) or FAP256 (CEP104) (24), yet the seeming importance of ARMC9 is not apparent in in vitro reconstitutions (5). Interestingly, we observed that although ARMC9 alone lacks ability to localize to cytoplasmic microtubules, it is recruited to microtubules by mCrescerin1. This recruitment in turn also appears to enhance mCrescerin1 microtubule affinity, as we observed a more distinct localization pattern in co-transfections (fig 2A). We have shown that ARMC9 is a dimer in solution, however our co-IP results suggest it does not need to dimerize to bind to mCrescerin1 (fig 2B-D) One potential mechanism accounting for the increased localization of mCrescerin1 to microtubules in the presence of ARMC9 might therefore involve previous microtubule bound mCrescerin1 to recruit ARMC9 to the lattice. ARMC9 could then dimerize which subsequently results in more mCrescerin1 recruitment, possibly explaining the observed more distinct localization pattern. Another possible mechanism might be that interaction with ARMC9 has a stabilizing effect on microtubule bound mCrescerin1. Next to ARMC9's function as a scaffold within the entire tip module, facilitating sufficient localization of mCrescerin1 to axonemal microtubules could be a possible additional role of ARMC9.

Interaction between ARMC9 and TOGARAM1 has previously been determined by Y2H screens to depend on TOG1 and TOG2 of TOGARAM1 and a C-terminal fragment of ARMC9 containing the CC and ARM domains (2). Through various co-IP assays, we narrowed down the interaction to be solely dependent on the TOG2 and ARM domains of mCrescerin1 and ARMC9 respectively (fig 2 D-F). We determined the CC domain of

ARMC9 to be necessary for dimerization but still observed co-precipitation of mCrescerin1 and ARMC9 ΔCC, which indicates that interaction is independent of the dimeric state of ARMC9. This was unexpected, as these findings contradict the aforementioned Y2H screen which suggested both the CC and ARM domain to be necessary for interaction. We sought to validate our co-IP findings by overexpressing the ARMC9 constructs used in the co-IP together with full-length mCrescerin1 in COS7 cells. Unexpectedly, we found that all ARMC9 constructs co-localized with mCrescerin1 to microtubules (although ARMC9 ΔARM to a lesser extent), contradicting our co-IP results (fig S2A). This discrepancy between our co-localization study and co-IP assay either suggest that ARMC9-mCrescerin1 interaction is rather robust and not strictly depended on the ARM domain, or may stem from additional cellular processes influencing ARMC9-mCrescerin1 interactions in the context of overexpression, rendering this experimental set-up unsuitable for studying protein-protein interactions.

In a Co-IP assay with ARMC9 JBTS point mutants in or close to the ARM domain and full length mCreserin1, only 1 of 4 ARMC9 mutants showed reduced co-precipitation (fig 3C). This could support the theory of robust interaction between the two proteins that only partially relies on the ARM domain. However, the effects on domain structure of these AMRC9 JBTS mutants was not determined, so it remains unclear to what extend they disrupt the binding surface. Armadillo repeat domains within the ARMC protein family are well-established interaction platforms (50). ARMC9 also localizes to basal bodies and is for example known to interact with transition zone protein CEP290 (2,24). Therefore, JBTS mutations in the ARM domain that do not disrupt interaction with mCrescerin1 might affect roles of ARMC9 outside of the tip module.

The binding site for ARMC9 on mCrescerin1 was narrowed down to TOG2 by co-IP assays with mCrescerin1 intra-HEAT loop point mutants previously predicted to disrupt tubulin binding capacity without effecting the overall domain fold (23). Furthermore, mCrescerin1 JBTS associated TOG2 point mutants completely abolish co-IP with ARMC9, which is in line with previous studies and highlights the importance of TOG2 for ARMC9 interaction (2) (fig 2E,F). Pairwise structural alignment of the intra-HEAT loop surface of TOG2 showed that it closely resembles the tubulin binding surface of Stu2 TOG1 and purified mCrescerin1 TOG2 shows polymerase activity in light scattering assays, suggesting TOG2 can bind to tubulin (23). Unpublished data from our lab and work by others however have shown that mCrescerin1 TOG2 is not needed for microtubule binding or the ability of mCrescerin1 to perform microtubule growth rescues in vitro (23). Taken together with our finding that mCrescerin1 interaction with ARMC9 is depended on TOG2, this suggests that TOG2 either converted to a different function or obtained an additional role as binding platform for interactions with other proteins.

CEP104 is recruited to growing microtubule plus-ends by EB, CCDC66 and CSPP1, through which it interacts with its SxIP motif and JR domain, respectively (5,15,16,51). Through co-IP assays, we confirmed the interaction of CEP104 with CCDC66 and CSPP1 and its dependency on the JR domain. We next performed transient transfection experiments in COS7 cells to test how the different functional domains of CEP104 contribute to its cellular localization in regard to microtubules. In line with previous findings, full length CEP104 co-localized with EB1 to growing cytoplasmic microtubule ends (5,19). CEP104 SXNN lost plus-end specificity and co-localization with EB1 (fig 5A). At high expression levels it still localized to cytoplasmic microtubules, in line with unpublished data from our lab suggesting CEP104 can bind to microtubules independently of EB3, CCDC66 or CSPP1. Interestingly, CEP104 ΔTOG still showed co-localization with microtubules, but similar to CEP104 SXNN, lost plus-end specificity and co-localization with EB1 (fig 5A). This localization pattern of CEP104 ΔTOG is counterintuitive for two reasons. Firstly, the purified TOG domain has previously been shown to bind to free tubulin (19). Though we note that free tubulin dimers are structurally different from the microtubule lattice. Secondly, in an overexpression experiment similar to ours, mutating the predicted tubulin binding surface of the TOG domain of Drosophila homologue DmCEP104, completely abolished localization to cytoplasmic microtubules (51). However, DmCEP104 differs from human CEP104 by

the lack of a SxIP motif (51). Accordingly, overexpressed DmCEP104 decorates cytoplasmic microtubule lattice without plus end specificity (51). One explanation for the loss of plus end specificity and EB1 co-localization of CEP104 ΔTOG that we observed might therefore be that the SxIP motif is no longer positioned correctly due to deleting the large TOG domain. Speculatively, the absence of an SxIP motif in DmCEP104 could possibly be connected to the different contributions of the TOG domain to lattice binding in both homologues.

As our results suggest that the TOG domain of human CEP104 is not necessary for microtubule lattice association, the question arises if a different functional domain facilitates this interaction. Possibly due to the strong co-localization with EB1 of CEP104 full length, ΔJR and ΔZNF, we did not observe EB independent or plus-end unspecific lattice localization in our transient transfection experiments. Therefore, we would not be able to have observed possible loss of lattice binding for either CEP104 ΔZNF or ΔJR if it was present. Endogenous expression levels of CCDC66 and CSPP1 are low, and therefore unlikely to be able to influence CEP104 localization in this experimental setup. In conclusion, further studies need to be done to determine how association of human CEP104 with the microtubule lattice independent of EBs is facilitated. Live cell imaging could provide more insight, as difference between microtubule plus end localization and EB mediated tip tracking becomes more pronounced.

A previous study determined direct interaction between ARMC9 and CCDC66 (2), which we confirmed for the full length proteins with co-IP (fig 1B). However, this interaction is not observed at in vitro reconstituted microtubules or in cells (5). This raises the question of whether the interaction is relevant for microtubule growth regulation by the tip module. Both CCDC66 and ARMC9 are thought to be tip module scaffolds as both us and others see that CCDC66 interacts with CEP104 and ARMC9 with mCrescerin1 and CSPP1, but they do not affect dynamics of in vitro reconstituted microtubules on their own(2,5,15,16). CEP104 has been shown to block microtubule growth in vitro upon sufficient accumulation at the microtubule end, and this behaviour can be potentiated by EB3, CSPP1 and CCDC66 (5). Blocking can be counteracted by mCrescerin1, but it needs to be determined if a direct interaction with CEP104 is required for this interplay (5). Through reciprocal co-IP assays, we showed that mCrescerin1 interacts through its central linker with the zinc finger of CEP104 (fig 5C,D). Assuming that direct interaction between CEP104 and mCrescerin1 is necessary for mCrescerin1 to counteract a block, the interaction between scaffolds CCDC66 and ARMC9 could be responsible for either recruiting and/or accumulating sufficient levels of both proteins at a similar site at the microtubule end, or for bringing both proteins in close proximity of each other.

Although indirect interactions between CSPP1 and mCrescerin1 have been shown by Latour et al. with co-IP experiments similar to ours (2), we did not observe these interactions. Notably, by working with overexpressed proteins from cell lysate, one can't discriminate between direct and indirect interaction. Also, observation of indirect interactions in co-IP assays in part relies on stringency of experimental conditions. The discrepancy between ours and Latour et al. co-IP assays could therefore be explained by more stringent experimental conditions. Whilst mCrescerin1 and CSPP1 show enhanced localization at microtubule ends, their binding sites lie on opposite sides of the microtubule wall. CSPP1 has been shown to localize to the microtubule lumen, and other TOG domain containing proteins similar to mCrescerin1, such as XMAP215 or CLASP family members, are known to bind to the microtubule lattice (6,43). It is therefore perhaps unsurprising that we did not see interaction between mCrescerin1 and CSPP1 in our co-IP assays. As mCrescerin1 and CSPP1 both interact with CEP104 and ARMC9, indirect interaction between these proteins is present (fig 2D-F and 4B-D). ARMC9 or CEP104 (or both) could potentially function as a bridge to connect CSPP1 and mCrescerin1 within the entire tip module complex.

Localization and function of tip module members is not restricted to the ciliary tip. Previous studies showed that various members localize to the centrosome region and previously mapped (in)direct protein-protein interactions have placed tip module proteins in different regulatory mechanisms, not restricted to the

primary cilia tip (14–16,26,28,29,51) (fig 7B). Namely, CEP104 has been shown to directly interact with CEP97 and CP110 at centriolar distal tips. This interaction is important for initiation of centrosome elongation in ciliogenesis and in Drosophila for the regulation of centriole length (51). CSPP1 is a core centrosome-component and is functionally linked to the control of G1 to S-phase progression, formation of spindle poles and contributes in cytokinesis (25,26,47,52). Lastly, CCDC66 plays important roles in centriolar satellite organization and cilia formation (16,28). Hence, further studies analysing the tip module proteins in the context of other regulatory mechanisms and investigating their potential role in regulating microtubule dynamics at other cellular locations, could contribute to a deeper understanding of the function of the tip module. Additionally, elucidating the bigger protein interaction network surrounding the axoneme could give further insights into how a stable axoneme is formed and maintained, especially in different stages of cilia assembly and disassembly.

To conclude, our findings add to the existing theory that ciliary tips are kept in shape by protein complexes that span both the inner and the outer microtubule surface (5,6). Such arrangement might be important in the regulation of various signalling pathways, such as Hedgehog signalling, which function depends on the state of the ciliary tip and it's dysregulation underlies ciliopathies (1,53,54). Indeed, JBTS associated point mutants disrupt specific interactions, highlighting the biological relevance of interactions within the tip module.

Materials and methods

Molecular cloning

All Joubert syndrome mutations and domain deletions were cloned from full length protein constructs described previously (5) in modified pEGFP-C1, pEGFP-N1 or pmCherry-C1 vectors containing a twin-Strep tag. A complete overview of all constructs can be found in table 2.

Mutations were cloned trough site directed mutagenesis with Phusion™ High–Fidelity DNA Polymerase (ThermoScientific) following company protocol with primers from IDT™ (table 2). Template DNA was removed by incubating total volume of PCR reaction with 1U DPN1 (ThermoScientific) for 1 hour at 37 ^{0}C followed by (gel) purification with Wizard PCR cleanup kit (Promega). DNA concentration was determined using a nanodrop (Spectrophotometer ND-1000, ISOGEN). 100 ng of purified linear PCR product was sequentially phosphorylated with 1U PNK (Thermofisher) for 15 min at 37 ^{0}C and ligated with 0.5 U T4 ligase for 1 hour at room temperature. DNA was amplified through heat shock transformation into competent DH10β. Plasmids were isolated with QIAprep Spin Miniprep Kit following company protocol. Cloned constructs were confirmed by sanger sequencing (Macrogen) and purified with PureLink™ HiPure Plasmid Filter Maxiprep Kit (ThermoScientific).

Cut and paste cloning to swap various constructs between previously named expression vectors was performed with FastDigest™ enzymes (ThermoScientific) following company protocol and downstream processing was performed as described previously.

Cell culture and transient transfections

HEK293T and COS7 cells were cultured in DMEM (Capricorn) and IMCD3 cells in 1:1 DMEM:F12 (Gibco), both supplemented with 10% fetal calf serum (FCS) (GE Healthcare Life Sciences) and 1% (v/v) penicillin/streptomycin (complete medium). Cells were incubated at 37°C with 5% CO_2 and routinely checked for mycoplasma contamination using the MycoAlertTM Mycoplasma Detection Kit (Lonza).

COS7 cells were transiently transfected with FuGENE6 (Promega) and 0.5 – 2 µG plasmid DNA of various constructs in pEGFP-C1 or pmCherry-C1 vectors in a 3:1 ratio. Medium was refreshed 6 hours after transfection. IMCD3 cells were transfected with 1 µG DNA and lipofectamine^{tm} 2000 (ThermoScientific) in a

1:3 ratio, following serum starvation for 24H in serum free 1:1 DMEM:F12 (Gibco) supplemented with 1% (v/v) penicillin/ streptomycin. IMCD3 cells were recovered in complete 1:1 DMEM:F12 just before transfection and medium was exchanged again 4H after addition of transfection mixtures to remove lipofectamine^{tm} 2000. HEK293T cells were transiently transfected with polyethyleneimine (Polysciences) diluted in F10 (Biowest) and 10 – 15 µG plasmid DNA of various constructs in pEGFP-C1 or pmCherry-C1 vectors in a 3:1 ratio. Medium was refreshed with complete 1:1 DMEM:F10 (Capricorn, Biowest) just before addition of transfection mixtures.

Immunofluorescent staining

COS7 and IMCD3 cells were seeded on 12-16 mm cover slips (Epredia) at 20% confluency and transiently transfected 24H later as described previously with 0.5 – 2 µG plasmid DNA. Cells were fixed 24H post transfection with -20°C MeOH for 5 min at -20 °C or with prewarmed 4% PFA – 4% sucrose for 12 min at room temperature and rehydrated for 10 min in 1x PBS. Cells were permeabilized for 2 min with 0.15% Triton-X in 1x PBS, washed 3 times for 5 min with wash buffer (0.05% Tween-20 in 1x PBS) and blocked for 45 min with blocking buffer (2% bovine serum albumin (BSA) in wash buffer). Fixed cells were sequentially stained with primary antibodies diluted in blocking buffer, washed 3 times for 5 min with wash buffer and stained with secondary antibodies diluted in wash buffer, both for 1 hour shaking at room temperature (table 3). After staining, cells were washed, dried with 96% ethanol and on tissue paper and mounted in vectashield (Vector laboratories) with or without DAPI on microscopy slides (Epredia). All slides were stored at +4 ^{0}C.

Co-immunoprecipitation assays

Hek293T cells were seeded in 10 cm^2 culture dishes at 30% confluency in complete 1:1 DMEM:F10 (Capricorn, Biowest) 24H prior to transfection as described previously. Co-IP was performed with ChromoTek GFP-Trap® Magnetic particles M-270 (Proteintech) following company protocol with company advised buffers. In brief, 24h post transfection, cells were harvested in 1x PBS and lysed for 30 min on ice in 200 µl lysis buffer (10 mM Tris HCl pH 7.5, 150 mM NaCl, 0.5 mM EDTA, 0.5% IGEPAL CA-630) supplemented with EDTA free protease inhibitor cocktail (Roche) and PhosSTOP™ phosphatase inhibitor cocktail (Roche). Lysate was cleared by 20 min centrifugation at +4 ^{0}C at 17,000x g and diluted with 300 µL dilution buffer (10 mM Tris HCl pH 7.5, 150 mM NaCl, 0.5 mM EDTA) supplemented with EDTA free protease inhibitor cocktail(Roche) and PhosSTOP™ phosphatase inhibitor cocktail (Roche) per sample. Diluted lysate was incubated rotating end-over-end for 45 min with in wash buffer equilibrated beads. Beads were washed four times with 500 µL wash buffer (10 mM Tris HCl pH 7.5, 150 mM NaCl, 0.5 mM EDTA, 0.05% IGEPAL CA-630) and protein was eluted in 80 µL 2x Laemmli sample buffer (0.125M tris HCl, 20% glycerol, 10% 2-mercaptoethanol,0.02% Bromophenol blue, 0.2M DTT) following heating at 95 ^{0}C for 5 min. All steps prior to elution were performed at +4 ^{0}C and all reagents and samples were kept on ice.

Western blot for analyzing Co-IP results

Protein samples were prepared in 2x Laemmli sample buffer and boiled at 95 ^{0}C for 5 min. Prepared samples were run on 8% SDS-page gel and blotted onto Amersham Protran Premium 0.45 NC nitrocellulose membrane (Cytiva) by wet transfer at 37 constant volts overnight at 4 ^{0}C in transfer buffer (0.2M tris-HCl, 2M glycine, 10% MeOH and 0.01% SDS), or by semi-dry transfer for 1H at 0.15 constant Ampère in transfer buffer (0.2M tris-HCl, 2M glycine, 10% MeOH). Membranes were blocked in blocking buffer (2% BSA diluted in 1x PBS 0.05% Tween-20) for 1 hour and sequentially incubated with primary antibodies and secondary antibodies (table 3) diluted in blocking buffer for 1 hour rotating at room temperature (primary and secondary antibodies) or overnight at +4 C^0 (primary antibodies only). Blots were thoroughly washed in between and after incubation with antibodies with wash buffer (1x PBS 0.05% Tween-20) and imaged with Odyssey® CLx Infrared Imaging System (LI-COR biosciences) at various exposure times. For co-IP assays with JBTS associated tip module protein variants, reduction in co-precipitation was analysed in FIJI by first normalizing signal of prey to the signal of corresponding bait, followed by normalizing co-IP to corresponding

input band. Analysis was performed using Graphpad Prism 9 and highest signal value was used to normalize data to 1.

Single molecule counting

HEK293T cells were seeded at 30% in 15 cm^2 culture dishes one day prior to transfection with 30 µG full length ARMC9 and ARMC9 ΔCC in pEGFP-C1 StrepII vector with polyethyleneimine (Polysciences) as described previously. 24H post transfection, cells were harvested in 1x PBS and lysed for 15 min on ice in 50 µL cold lysis buffer (50 mM HEPES, 300 mM NaCl, 1 mM MgCl2, 1 mM DTT, 0.5%, Triton X-100, pH 7.4) supplemented with EDTA free protease inhibitor cocktail (Roche). Lysate was cleared by centrifugation in table top centrifuge for 20 min at 17,000x g, snap-frozen in liquid nitrogen and stored at -80 ^{0}C. Square, medium RF level plasma-cleaned (Expanded plasma cleaner PDC-002, Harrick Plasma) glass coverslips (Epredia) were attached on slides (Epredia) with double sided tape to create three chambers. Chambers were pre-wetted with 1x PBS after which diluted cell lysate, purified GFP or GFP tagged EB3 were flown in. Purified GFP-EB3 was a gift (Montenegro Gouveia et al.,2010) and GFP was purified in-house by another lab member. Chambers were sealed with vacuum grease and slides were immediately imaged with TIRF microscopy. Detection and quantification of single molecules were performed using Detection of Molecules (DoM) plugin v.1.2.5 for ImageJ (*https://github.com/UU-cellbiology/DoM_Utrecht*). Analysis was performed using Graphpad Prism 9.

Microscopy

Widefield microscopy

Fixed and stained cells were imaged on Nikon Eclipse Ni Upright microscope suitable for widefield fluorescence illumination. This microscope has a Nikon DS-Qi2 camera (Nikon), an Intensilight C-HGFI precentered fibre illuminator (Nikon), ET-DAPI, ET-EGFP and ET-mCherry filters (Chroma) and a Plan Apo Lambda 60x NA 1.4 oil objective (Nikon). The set-up is controlled by Nikon NIS Br software. Of the presented images, brightness and contrast were adjusted in FIJI.

Confocal microscopy

Fixed and stained cells were imaged on Zeiss LSM700 AxioObserver Z1 confocal microscope. This microscope is equipped with plan-Apochromat 63x/ 1.40 oil DIC (WD=0.19 mm) objective which was used form imaging. It has laser lines; 405nm, 488nm, 555nm and 633 nm and microscope set-up is controlled ZEN 2011 software. Of the presented images, brightness and contrast were adjusted in FIJI.

Tirf microscopy

TIRF microscopy was performed on a iLas2 TIRF system previously described by van den Berg et al. (6). Briefly, we used an inverted research microscope Nikon Eclipse Ti-E (Nikon) with the perfect focus system (Nikon), equipped with Nikon CFI Apo TIRF 100 × 1.49 N.A. oil objective (Nikon) and controlled with MetaMorph 7.10.2.240 software (Molecular Devices). The microscope was equipped with TIRF-E motorized TIRF illuminator modified by Gataca Systems (France). For excitation, 490 nm 150 mW Vortran Stradus 488 laser (Vortran) laser was used. We used ET-GFP 49002 filter set (Chroma) for imaging of proteins tagged with GFP. Fluorescence was detected using an EMCCD Evolve 512 camera (Roper Scientific) without an additional lens.

Table 2 *DNA constructs*

Construct	***Type***	***Primers (5' – 3')***	***Source***
ARMC9			
strepII-GFP/mCh-ARMC9 FL	Full length	NA	*(Van den Berg et al, 2023)* (5)
StrepII-GFP/mCh-ARMC9 ΔlisH	Domain deletion (del. AA 6-37)	**Fwd:**GGAAAACCATTGTGTAAAACAGTAG **Rvs:** AGCCAGAATGTCCCCAGA	This study
StrepII-GFP/mCh-ARMC9 ΔCC	Domain deletion (del. AA 203-229)	**Fwd:** TACAATAAGATCCAGGCC **Rvs:** TCCATTCTCCTTATATATTGTTAAAAG	This study
StrepII-GFP/mCh-ARMC9 ΔArmadillo	Domain deletion (del. AA 450- 571)	**Fwd:** GAAGAGCTACCAGATGGTGTTCTTGA ATCTGATGATG **Rvs:** TGTCTGCAGCGGGCGCCT	This study
StrepII-GFP/mCh-ARMC9 R86*	JBTS, truncation before CC (del. AA 86-664)	**Fwd:**TAAGTCGACGGTACCGCG **Rvs:** GATGGAACTTGAAATGTGCTCC	This study
StrepII-GFP/mCh-ARMC9 R298*	JBTS, truncation before ARM (del. AA 298-664)	**Fwd:** TAAGTCGACGGTACCGCG **Rvs:** TAACATGGTGGATGCCGTC	This study
StrepII-GFP/mCh-ARMC9 G492R	JBTS, mutation in ARM	**Fwd:** CCGCAGCACAaGGAAGAACAT **Rvs:** AGGCAGAGGTTCATGAGCAAAG	This study
StrepII-GFP/mCh-ARMC9 R445C	JBTS, mutation in linker between CC and ARM	**Fwd:** CAGTCTCAGGtgcCCGCTGCAGA **Rvs:** AACTTCTGCAGGGCCCCAAG	This study
StrepII-GFP/mCh-ARMC9 P520L	JBTS, mutation in ARM	**Fwd:** GAGATACAGCtGTATGTGAATG **Rvs:** ATGGTTTTCATGGCCAAG	This study
mCrescerin1			
StrepII-GFP/mCh-mCrescerin1 FL	Full length	NA	*(Van den Berg et al, 2023)* (5)
StrepII-GFP/mCh-mCrescerin1 P109E	Mutation in first intra heat loop of TOG1	**Fwd:** CGCACCGGATGAGTCCGAGGCGT **Rvs:** GTGCGCAGGAGTAGA	Gifted by Slep lab *(Das et al., 2015)* (23)
StrepII-GFP/mCh-mCrescerin1 Y364E	Mutation in first intra heat loop of TOG2	NA	Gifted by Slep lab *(Das et al., 2015)* (23)
StrepII-GFP/mCh-mCrescerin1 P109E and Y264E	Mutation in first intra heat loop of TOG1 and TOG2	NA	Gifted by Slep lab *(Das et al., 2015)* (23)
StrepII-GFP/mCh-	Truncation	NA	Other lab member, unpublished

mCrescerin1 TOG 1+2			
StrepII-GFP/mCh-mCrescerin1 TOG 3+4	Truncation	NA	Other lab member, unpublished
StrepII-GFP/mCh-mCrescerin1 Linker + TOG 3+4	Truncation	NA	Other lab member, unpublished
StrepII-GFP/mCh-mCrescerin1 Q360*	JBTS, truncation in TOG2	**Fwd:** TAAGTCGACGGTACCGCG **Rvs:** ATCCAACAGTCTTGCATGGAG	This study
StrepII-GFP/mCh-mCrescerin1 A371D	JBTS, mutation in TOG2	**Fwd:** AGGACTCAGGaTGTTGAAGAAC **Rvs:** GTTTTTATAATCTTCCTGATCCAACA	This study
StrepII-GFP/mCh-mCrescerin1 L373P	JBTS, mutation in TOG2	**Fwd:** TGTTGAAGAAccaAAGCAGTTGC **Rvs:** GCCTGAGTCCTGTTTTTATAATC	This study
StrepII-GFP/mCh-mCrescerin1 R1311C	JBTS, mutation in TOG3	**Fwd:** GAAAAATTTAtgcTCTGGAGTGTC **Rvs:** TTTCACCTCTTGAACTACTGC	This study
CEP104			
StrepII-GFP/mCh-CEP104 FL	Full length	NA	*(Van den Berg et al, 2023)* (5)
StrepII-GFP/mCh-CEP104 ΔJR	Domain deletion	NA	Other lab member, unpublished
StrepII-GFP/mCh-CEP104 ΔTOG	Domain deletion	**Fwd:** GCTACAGATGCTGAGATGAG **Rvs:** TAACATGCCTCCCCTCCG	This study
StrepII-GFP/mCh-CEP104 ΔZNF	Domain deletion	NA	Other lab member, unpublished
StrepII-GFP/mCh-CEP104 SxNN	Point mutation	NA	Other lab member, unpublished
StrepII-GFP/mCh-CEP104 R111W	JBTS, mutation in JR	**Fwd:** TTGCAAAGCCtGGGAACTAAA **Rvs:** CCTGTCTTTTCATTATCACAG	This study (cloned by other lab member)

Table 3 *Primary and secondary antibodies*

Antibody	Used dilution	Source	Identifier
Immunofluorescent staining			
anti α-tubulin AA345, mouse	1:300	Gifted by Paul Guichard	NA
anti β-tubulin AA344, mouse	1:300	Gifted by Paul Guichard	NA
Anti EB1, clone 11B11, rat	1:20	Akhmanova lab	NA
Anti tubulin- α gL1/2 (tyrosinated)	1:300/ 1:400	Pierce/ thermos scientific	MA1-80017
Anti tubulin-acylated (Lys40)	1:400	Bioke	5335S
Goat anti-Mouse IgG (H+L) Cross-Adsorbed Secondary Antibody, Alexa Fluor™ 647	1:300	Thermofisher scientific/ Invitrogen	A-21235
Goat anti-Rat IgG (H+L) Cross-Adsorbed Secondary Antibody, Alexa Fluor™ 594	1:500	Thermofisher scientific/ Invitrogen	A-11007
Goat anti-Rat IgG (H+L) Cross-Adsorbed Secondary Antibody, Alexa Fluor™ 647	1:400	Thermofisher scientific/ Invitrogen	A-21247
Goat anti-Rabbit IgG (H+L) Cross-Adsorbed Secondary Antibody, Alexa Fluor™ 405	1:400	Thermofisher scientific/ Invitrogen	A-31556
Immunoblotting			
anti RFP Antibody , rabbit polyclonal	1:2000	Rockland immunochemicals	600-401-379
Anti-Green Fluorescent Protein (GFP) antibody, mouse monoclonal	1:2000	Sigma-Aldrich	G1546
IRDye® 800CW Donkey anti-Mouse IgG (H + L)	1:10.000	LI-COR biosciences	926-32212
IRDye® 680CW Donkey anti-Rabbit IgG (H + L)	1:10.000	LI-COR biosciences	926-68072

Acknowledgments

I thank Anna Akhmanova and Harriet Saunders for setting up this interesting project, supplying materials and equipment and for providing guidance and advice throughout the internship. In addition, I want to especially thank Harriet Saunders for the great daily supervision and the guidance both during the practical work and writing of this report. Furthermore, I want to thank all other Akhmanova lab members and the rest of the cell biology department for providing a good working environment and additional assistance with lab work. I thank the Roepman lab for providing us with the IMCD3 cell line, communicating the unpublished CEP104 R111W JBTS variant and for providing plasmids containing cDNA of full-length tip module proteins. I thank the Slep lab for providing us with DNA constructs of mCrescerin1 intra-HEAT loop point mutants. Lastly, I want to thank friends and fellow students for support and additional help and feedback during my internship and writing of the report.

References

1. Bettencourt-Dias M, Hildebrandt F, Pellman D, Woods G, Godinho SA. Centrosomes and cilia in human disease. Trends in Genetics. 2011 Aug;27(8):307–15.

2. Latour BL, Van De Weghe JC, Rusterholz TD, Letteboer SJ, Gomez A, Shaheen R, et al. Dysfunction of the ciliary ARMC9/TOGARAM1 protein module causes Joubert syndrome. J Clin Invest. 2020 Aug 3;130(8):4423–39.

3. Wang W, Jack BM, Wang HH, Kavanaugh MA, Maser RL, Tran PV. Intraflagellar Transport Proteins as Regulators of Primary Cilia Length. Frontiers in Cell and Developmental Biology. 2021;9:661350.

4. Keeling J, Tsiokas L, Maskey D. Cellular Mechanisms of Ciliary Length Control. Cells. 2016 Mar;5(1):6.

5. Van den Berg C. Tip support. 2023.

6. van den Berg CM, Volkov VA, Schnorrenberg S, Huang Z, Stecker KE, Grigoriev I, et al. CSPP1 stabilizes growing microtubule ends and damaged lattices from the luminal side. J Cell Biol. 2023 Apr 3;222(4):e202208062.

7. Conkar D, Firat-Karalar EN. Microtubule-associated proteins and emerging links to primary cilium structure, assembly, maintenance, and disassembly. The FEBS Journal. 2021;288(3):786–98.

8. Klena N, Pigino G. Structural Biology of Cilia and Intraflagellar Transport. Annual Review of Cell and Developmental Biology. 2022;38(1):103–23.

9. Bettencourt-Dias M, Hildebrandt F, Pellman D, Woods G, Godinho SA. Centrosomes and cilia in human disease. Trends in Genetics. 2011 Aug 1;27(8):307–15.

10. Kiesel P, Alvarez Viar G, Tsoy N, Maraspini R, Gorilak P, Varga V, et al. The molecular structure of mammalian primary cilia revealed by cryo-electron tomography. Nat Struct Mol Biol. 2020 Dec;27(12):1115–24.

11. Deretic J, Odabasi E, Firat-Karalar EN. The multifaceted roles of microtubule-associated proteins in the primary cilium and ciliopathies. Journal of Cell Science. 2023 Dec 1;136(23):jcs261148.

12. Marshall WF. The cell biological basis of ciliary disease. The Journal of Cell Biology. 2008 Jan 14;180(1):17–21.

13. Avasthi P, Marshall WF. Stages of Ciliogenesis and Regulation of Ciliary Length. Differentiation. 2012 Feb;83(2):S30–42.

14. Breslow DK, Hoogendoorn S, Kopp AR, Morgens DW, Vu BK, Kennedy MC, et al. A CRISPR-based screen for Hedgehog signaling provides insights into ciliary function and ciliopathies. Nat Genet. 2018 Mar;50(3):460–71.

15. Frikstad KAM, Molinari E, Thoresen M, Ramsbottom SA, Hughes F, Letteboer SJF, et al. A CEP104-CSPP1 Complex Is Required for Formation of Primary Cilia Competent in Hedgehog Signaling. Cell Rep. 2019 Aug 13;28(7):1907-1922.e6.

16. Odabasi E, Conkar D, Deretic J, Batman U, Frikstad KAM, Patzke S, et al. CCDC66 regulates primary cilium length and signaling via interactions with transition zone and axonemal proteins. J Cell Sci. 2023 Feb 1;136(3):jcs260327.

17. Brancati F, Dallapiccola B, Valente EM. Joubert Syndrome and related disorders. Orphanet J Rare Dis. 2010 Jul 8;5(1):20.

18. Al-Jassar C, Andreeva A, Barnabas DD, McLaughlin SH, Johnson CM, Yu M, et al. The Ciliopathy-Associated Cep104 Protein Interacts with Tubulin and Nek1 Kinase. Structure. 2017 Jan 3;25(1):146–56.

19. Rezabkova L, Kraatz SHW, Akhmanova A, Steinmetz MO, Kammerer RA. Biophysical and Structural Characterization of the Centriolar Protein Cep104 Interaction Network. J Biol Chem. 2016 Aug 26;291(35):18496–504.

20. Yamazoe T, Nagai T, Umeda S, Sugaya Y, Mizuno K. Roles of TOG and jelly-roll domains of centrosomal protein CEP104 in its functions in cilium elongation and Hedgehog signaling. J Biol Chem. 2020 Oct 23;295(43):14723–36.

21. Satish Tammana TV, Tammana D, Diener DR, Rosenbaum J. Centrosomal protein CEP104 (Chlamydomonas FAP256) moves to the ciliary tip during ciliary assembly. J Cell Sci. 2013 Nov 1;126(21):5018–29.

22. Oegema K, Whitfield WG, Alberts B. The cell cycle-dependent localization of the CP190 centrosomal protein is determined by the coordinate action of two separable domains. Journal of Cell Biology. 1995 Dec 1;131(5):1261–73.

23. Das A, Dickinson DJ, Wood CC, Goldstein B, Slep KC. Crescerin uses a TOG domain array to regulate microtubules in the primary cilium. Mol Biol Cell. 2015 Nov 15;26(23):4248–64.

24. Louka P, Vasudevan KK, Guha M, Joachimiak E, Wloga D, Tomasi RFX, et al. Proteins that control the geometry of microtubules at the ends of cilia. Journal of Cell Biology. 2018 Sep 14;217(12):4298–313.

25. Asiedu M, Wu D, Matsumura F, Wei Q. Centrosome/Spindle Pole–associated Protein Regulates Cytokinesis via Promoting the Recruitment of MyoGEF to the Central Spindle. Mol Biol Cell. 2009 Mar 1;20(5):1428–40.

26. Patzke S, Stokke T, Aasheim HC. CSPP and CSPP-L associate with centrosomes and microtubules and differently affect microtubule organization. Journal of Cellular Physiology. 2006;209(1):199–210.

27. Rai A, Liu T, Glauser S, Katrukha EA, Estévez-Gallego J, Rodríguez-García R, et al. Taxanes convert regions of perturbed microtubule growth into rescue sites. Nat Mater. 2020 Mar;19(3):355–65.

28. Conkar D, Culfa E, Odabasi E, Rauniyar N, Yates JR, Firat-Karalar EN. The centriolar satellite protein CCDC66 interacts with CEP290 and functions in cilium formation and trafficking. J Cell Sci. 2017 Apr 15;130(8):1450–62.

29. Van De Weghe JC, Rusterholz TDS, Latour B, Grout ME, Aldinger KA, Shaheen R, et al. Mutations in ARMC9, which Encodes a Basal Body Protein, Cause Joubert Syndrome in Humans and Ciliopathy Phenotypes in Zebrafish. The American Journal of Human Genetics. 2017 Jul 6;101(1):23–36.

30. Haycraft CJ, Banizs B, Aydin-Son Y, Zhang Q, Michaud EJ, Yoder BK. Gli2 and Gli3 Localize to Cilia and Require the Intraflagellar Transport Protein Polaris for Processing and Function. PLOS Genetics. 2005 okt;1(4):e53.

31. Jiang K, Toedt G, Montenegro Gouveia S, Davey NE, Hua S, van der Vaart B, et al. A Proteome-wide Screen for Mammalian SxIP Motif-Containing Microtubule Plus-End Tracking Proteins. Current Biology. 2012 Oct 9;22(19):1800–7.

32. Sun S, Fisher R, Bowser S, Pentecost B, Siu H. Three-dimensional architecture of epithelial primary cilia. 116(19):9370–9.

33. Sternemalm J, Russnes HG, Zhao X, Risberg B, Nord S, Caldas C, et al. Nuclear CSPP1 expression defined subtypes of basal-like breast cancer. Br J Cancer. 2014 Jul;111(2):326–38.

34. Batman U, Deretic J, Firat-Karalar EN. The ciliopathy protein CCDC66 controls mitotic progression and cytokinesis by promoting microtubule nucleation and organization. PLOS Biology. 2022 Jul 18;20(7):e3001708.

35. Truebestein L, Leonard TA. Coiled-coils: The long and short of it. Bioessays. 2016 Sep;38(9):903–16.

36. Farmer VJ, Zanic M. TOG-domain proteins. Curr Biol. 2021 May 24;31(10):R499–501.

37. Zhao B, Pritchard JR. Evolution of the nonsense-mediated decay pathway is associated with decreased cytolytic immune infiltration. PLOS Computational Biology. 2019 okt;15(10):e1007467.

38. Richards JE, Hawley RS. Chapter 5 - We Are All Mutants: How Mutation Alters Function. In: Richards JE, Hawley RS, editors. The Human Genome (Third Edition) [Internet]. San Diego: Academic Press; 2011 [cited 2023 Dec 5]. p. 143–95. Available from: https://www.sciencedirect.com/science/article/pii/B9780080918655000059

39. Li B, Krishnan VG, Mort ME, Xin F, Kamati KK, Cooper DN, et al. Automated inference of molecular mechanisms of disease from amino acid substitutions. Bioinformatics. 2009 Nov 1;25(21):2744–50.

40. Wang H, Luo G, Hu W, Mei J, Shen Y, Wang M, et al. Whole Exome Sequencing Identified Novel ARMC9 Variations in Two Cases With Joubert Syndrome. Frontiers in Genetics. 2022;13:817153.

41. Srour M, Hamdan F, McKnight D, Davis E, Mandel H, Schwartzentruber J, et al. Joubert Syndrome in French Canadians and Identification of Mutations in CEP104. American journal of human genetics. 2015 Oct 19;97.

42. Luo M, Cao L, Cao Z, Ma S, Shen Y, Yang D, et al. Whole exome sequencing reveals novel CEP104 mutations in a Chinese patient with Joubert syndrome. Mol Genet Genomic Med. 2019 Oct 18;7(12):e1004.

43. Al-Bassam J, Chang F. Regulation of microtubule dynamics by TOG-domain proteins XMAP215/Dis1 and CLASP. Trends Cell Biol. 2011 Oct;21(10):604–14.

44. Shaheen R, Shamseldin HE, Loucks CM, Seidahmed MZ, Ansari S, Ibrahim Khalil M, et al. Mutations in CSPP1, encoding a core centrosomal protein, cause a range of ciliopathy phenotypes in humans. Am J Hum Genet. 2014 Jan 2;94(1):73–9.

45. Tsang WY, Dynlacht BD. CP110 and its network of partners coordinately regulate cilia assembly. Cilia. 2013 Jul 26;2(1):9.

46. Kim J, Krishnaswami SR, Gleeson JG. CEP290 interacts with the centriolar satellite component PCM-1 and is required for Rab8 localization to the primary cilium. Hum Mol Genet. 2008 Dec 1;17(23):3796–805.

47. Patzke S, Redick S, Warsame A, Murga-Zamalloa CA, Khanna H, Doxsey S, et al. CSPP Is a Ciliary Protein Interacting with Nephrocystin 8 and Required for Cilia Formation. MBoC. 2010 Aug;21(15):2555–67.

48. Gupta GD, Coyaud É, Gonçalves J, Mojarad BA, Liu Y, Wu Q, et al. A Dynamic Protein Interaction Landscape of the Human Centrosome-Cilium Interface. Cell. 2015 Dec 3;163(6):1484–99.

49. Saunders HAJ, Johnson-Schlitz DM, Jenkins BV, Volkert PJ, Yang SZ, Wildonger J. Acetylated α-tubulin K394 regulates microtubule stability to shape the growth of axon terminals. Current Biology. 2022 Feb;32(3):614-630.e5.

50. Huang Y, Jiang Z, Gao X, Luo P, Jiang X. ARMC Subfamily: Structures, Functions, Evolutions, Interactions, and Diseases. Frontiers in Molecular Biosciences. 2021;8:791597.

51. Ryniawec JM, Hannaford MR, Zibrat ME, Fagerstrom CJ, Galletta BJ, Aguirre SE, et al. Cep104 is a component of the centriole distal tip complex that regulates centriole growth and contributes to Drosophila spermiogenesis. Current Biology. 2023 Oct;33(19):4202-4216.e9.

52. Patzke S, Hauge H, Sioud M, Finne EF, Sivertsen EA, Delabie J, et al. Identification of a novel centrosome/microtubule-associated coiled-coil protein involved in cell-cycle progression and spindle organization. Oncogene. 2005 Feb;24(7):1159–73.

53. Andreu-Cervera A, Catala M, Schneider-Maunoury S. Cilia, ciliopathies and hedgehog-related forebrain developmental disorders. Neurobiol Dis. 2021 Mar;150:105236.

54. Reiter JF, Leroux MR. Genes and molecular pathways underpinning ciliopathies. Nat Rev Mol Cell Biol. 2017 Sep;18(9):533–47.

55. Akizu N, Silhavy JL, Rosti RO, Scott E, Fenstermaker AG, Schroth J, et al. Mutations in CSPP1 lead to classical Joubert syndrome. Am J Hum Genet. 2014 Jan 2;94(1):80–6.

56. Tuz K, Bachmann-Gagescu R, O'Day DR, Hua K, Isabella CR, Phelps IG, et al. Mutations in CSPP1 cause primary cilia abnormalities and Joubert syndrome with or without Jeune asphyxiating thoracic dystrophy. Am J Hum Genet. 2014 Jan 2;94(1):62–72.

57. CSPP1 - Centrosome and spindle pole associated protein 1 - Homo sapiens (Human) | UniProtKB | UniProt [Internet]. [cited 2023 Nov 30]. Available from: https://www.uniprot.org/uniprotkb/A0A7I2V5W3/entry

Supplemental figures

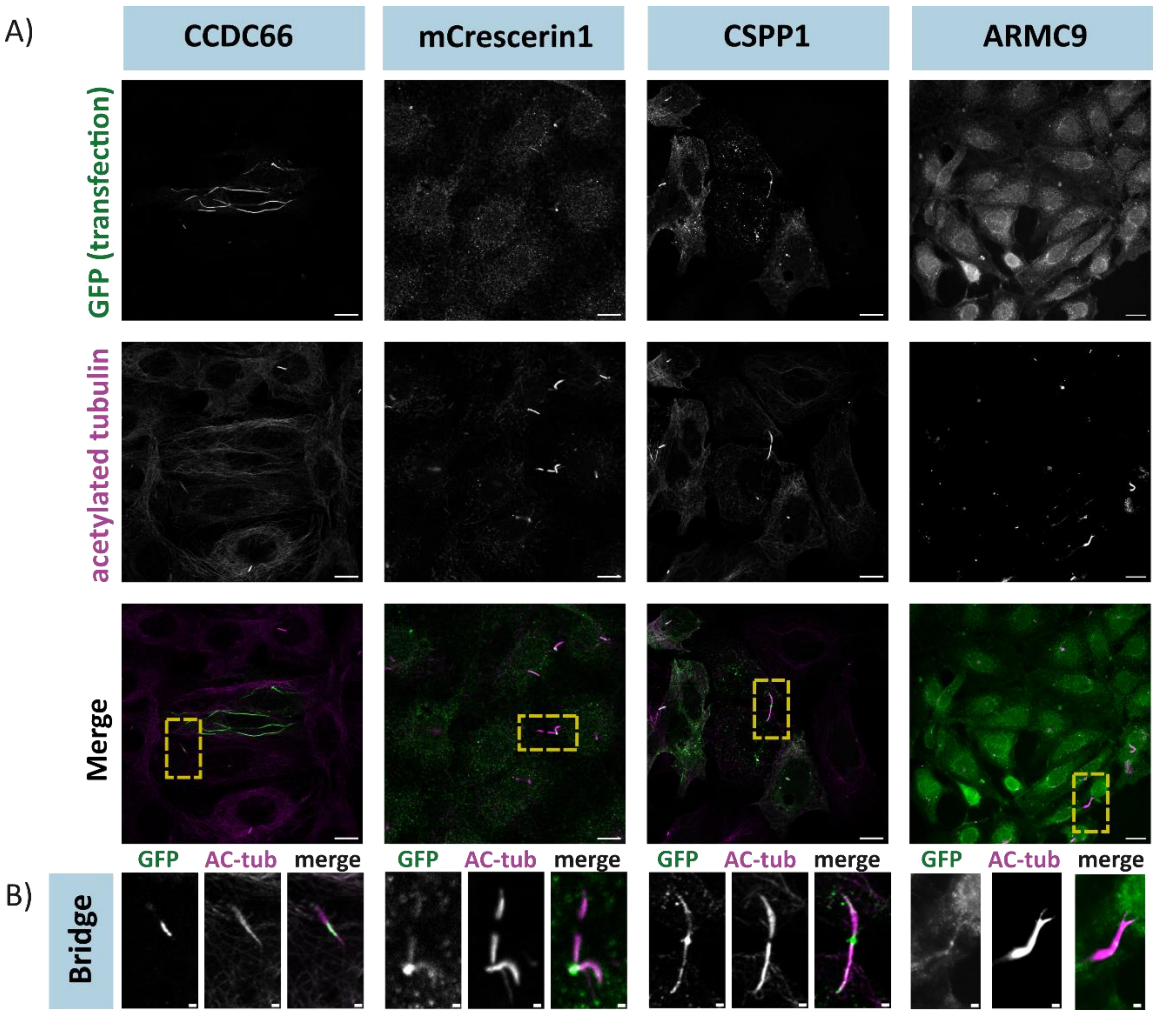

Supplemental figure S1 *A) Zeiss Lsm700 63x confocal fluorescence images (CSPP1, CCDC66 and mCrescerin1) or Nikon Eclipse Ni Upright 60x widefield image (ARMC9) of fixed murine inner medullary collecting duct (IMCD3) cells overexpressing GFP tagged full length: CCDC66 and CSPP1 or with immunostaining for endogenous TOGARAM1 or ARMC9. Primary cilia and microtubules are visualized by Immunostaining* for *acetylated tubulin and tyrosinated α-tubulin, respectively. Scale bar, 10 µm. (B) close-up of images displayed in 1A, showing cytoplasmic bridges. Scale bar, 1 µm.*

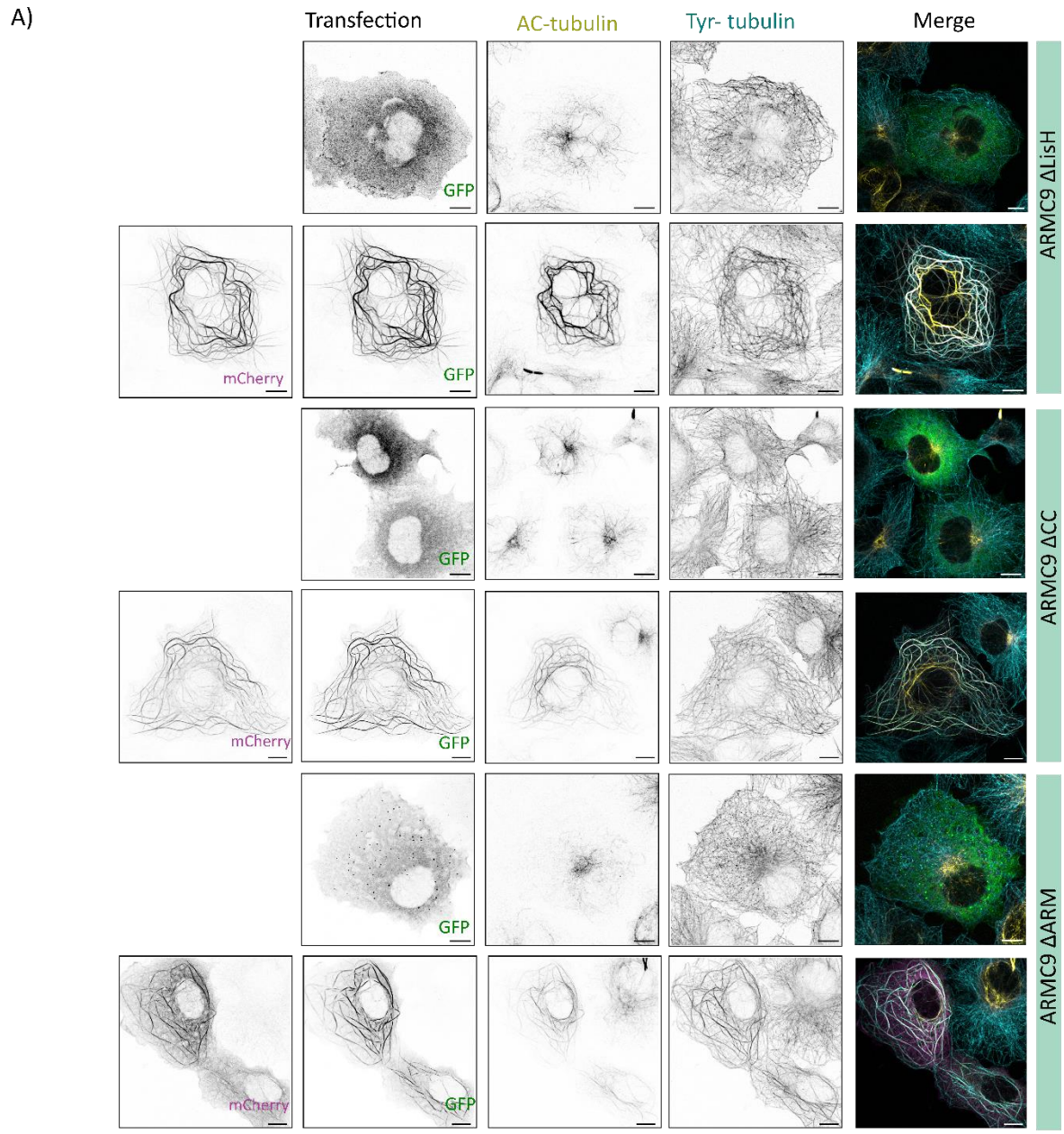
A)
Transfection
AC-tubulin
Tyr- tubulin
Merge
GFP
mCherry
ARMC9 ΔLisH
ARMC9 ΔCC
ARMC9 ΔARM

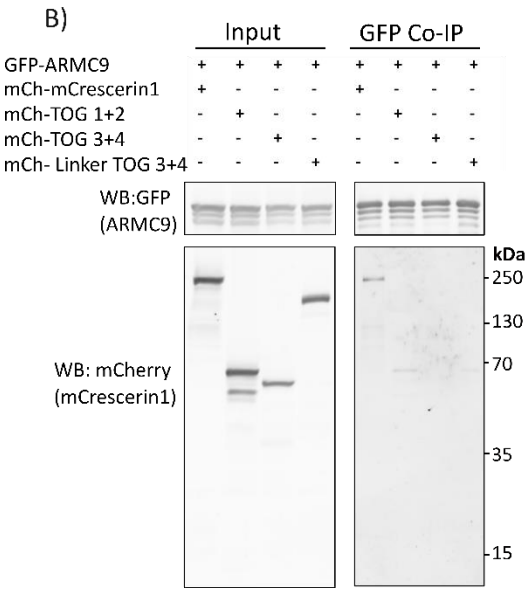
B)
Input
GFP Co-IP
GFP-ARMC9
mCh-mCrescerin1
mCh-TOG 1+2
mCh-TOG 3+4
mCh- Linker TOG 3+4
WB:GFP
(ARMC9)
WB: mCherry
(mCrescerin1)
kDa
250
130
70
35
15

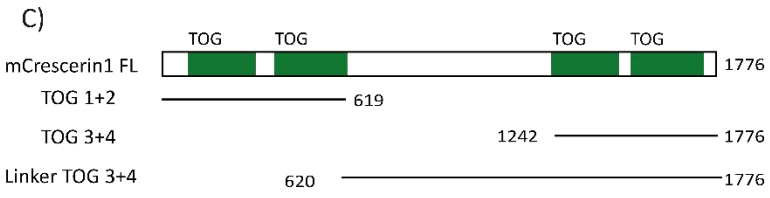
C)
TOG
TOG
TOG
TOG
mCrescerin1 FL
1776
TOG 1+2
619
TOG 3+4
1242
1776
Linker TOG 3+4
620
1776

Supplemental figure S2 *(A) Zeiss Lsm700 63x confocal fluorescence images of fixed COS7 cells overexpressing GFP tagged ARMC9 constructs: ΔLisH, ΔCC and ΔARM as single transfection or co-transfected with full length mCherry tagged mCrescerin1. Microtubules are visualized by immunostaining for acetylated tubulin and tyrosinated α-tubulin. Scale bar, 10 µm. (B) GFP co-IP of GFP tagged full length ARMC9 with mCherry tagged mCrescerin1 constructs: full length, TOG 1+2, TOG 3+5 and linker + TOG 3+4. WB analysis after GFP targeted immunoprecipitation indicated the presence of mCherry tagged mCrescerin1 FL and TOG 1+2 but the absence of TOG 3+4 and linker + TOG 3+4, confirming the dependency of the first 2 TOG domains for mCrescerin1-ARMC9 interaction* (2)*. (C) protein schematic of mCrescerin1 truncations.*

Supplemental table S1 *Gene variants in individuals with CSPP1 related JBTS, , domain annotations according to Uniprot database* (44,55–57)

Mutation	Functional domain	Pt. Identifier	source
652C>T (Q218*)	NA	MTI-136 and UW141-3 and -4	(Akizu et al., 2014) (55) (Tuz et al., 2014) (56)
2773C>T (R925*)	CC6	MTI-2109	(Akizu et al., 2014) (55)
448C>T (Q150*)	NA	MTI-2201	(Akizu et al., 2014) (55)
950+1G>C (splice)	NA	MTI-159 and UW137-3	(Akizu et al., 2014) (55) (Tuz et al., 2014) (56)
2243_2244delAA/ 2244_2245delAA (E750G fs*30)	NA	MTI-1342, UW097-3 and UW097-6	(Akizu et al., 2014) (55) (Tuz et al., 2014) (56)
2260C>T (R754*)	NA	MTI-1561, UW128-3	(Akizu et al, 2014) (55) (Tuz et al., 2014) (56)
457delA (R153G fs*35)	NA	MTI-1561, UW128-3	(Akizu et al., 2014) (55) (Tuz et al., 2014) (56)
2320C>T (R774*)	NA	JS-1701 (homozygous)	(Tuz et al., 2014) (56)
2708delA (N903M fs*2)	NA	UW035-3 (homozygous)	(Tuz et al., 2014) (56)
2280delA (E761K fs*35)	NA	UW097-3, UW097-6	(Tuz et al., 2014) (56)
3211_3212 insA (Y1071*)	NA	UW123-3, UW124-3, UW148-3	(Tuz et al., 2014) (56)
2953+1G>A (splice)	NA	UW123-3, UW124-3, UW148-3	(Tuz et al., 2014) (56)
2448_2454 dupAGAAGAA (E818R fs*7)	NA	UW127-3 (homozygous)	(Tuz et al., 2014) (56)
658 C>T (R220*)	NA	UW129-3, UW129-4	(Tuz et al., 2014) (56)
2527-2528 delAT (M843G fs*25)	NA	UW129-3, UW129-4, UW130-3 (homozygous), UW147-3 (homozygous)	(Tuz et al., 2014) (56)
3205+1G>A (splice)	NA	UW137-3, MTI-149	(Akizu et al., 2014) (55) (Tuz et al., 2014) (56)
1214G>A (R405Q fs*2)	NA	UW141-3 and -4	(Tuz et al., 2014) (56)
1132 C>T (R378*)	NA	UW143-3, UW143-4	(Tuz et al., 2014) (56)
2441-2444 del AGAA (K814R fs*21)	NA	UW143-3 and -4	(Tuz et al., 2014) (56)
2448_2454 delAGAAGAA (E817K fs*17)	NA	UW151-3 (homozygous)	(Tuz et al., 2014) (56)
2244-2247 del AAGA (E750K fr*7)	NA	NA	(Shaheen et al., 2014) (44)

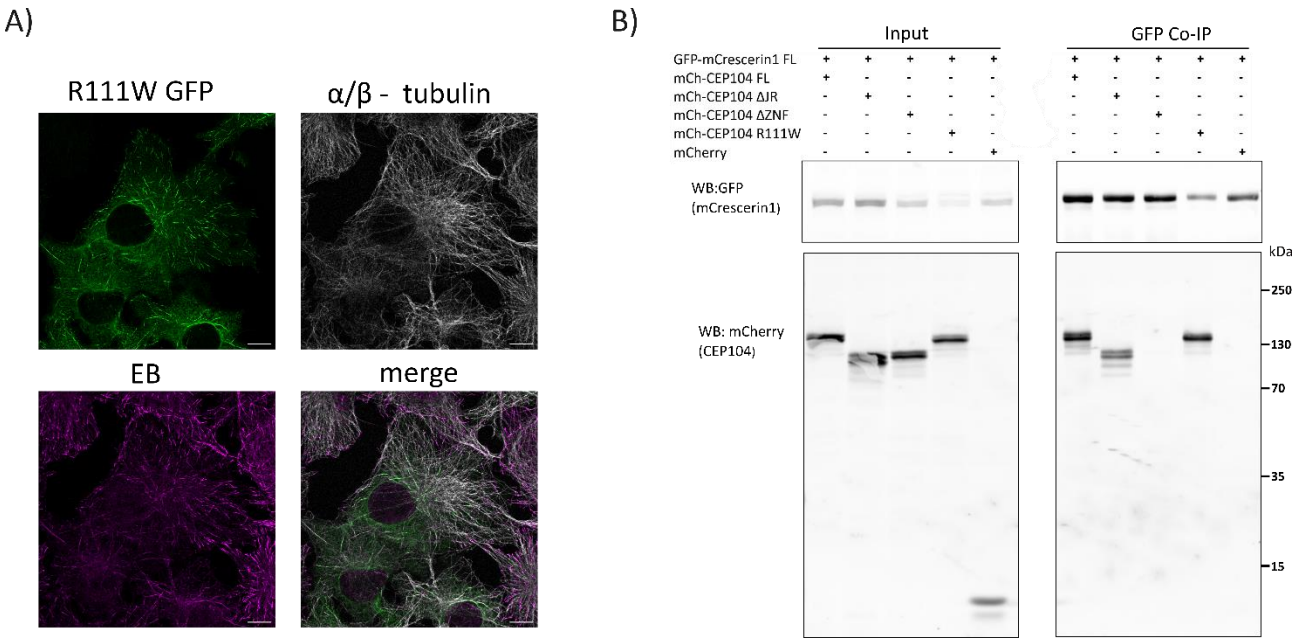

Supplemental figure S3 *(A) Zeiss Lsm700 63x confocal fluorescence images of fixed COS7 cells overexpressing GFP tagged CEP104 R111W. Immunostaining for EB1 and α/β-tubulin. Scale bar, 10 µm. (B) GFP co-IP of GFP tagged full length mCrescerin1 with mCherry tagged CEP104 constructs: full length, ΔJR, ΔZNF and R111W. WB analysis after GFP targeted immunoprecipitation indicated the presence of mCherry tagged CEP104 FL, ΔJR and R111W and the absence of ΔZNF and mCherry, which where included as negative controls.*

Layman summary

Primary cilia are hair-like structures that can be found on the surface of many different types of cells. They function as signalling centres by decoding various mechanical and chemical stimuli that a cell receives from neighbouring cells and it's environment. They can therefore be viewed as cellular antennas. Primary cilia provide a way for cells to communicate with each other and coordinate specific behaviours, such as differentiation. Many different proteins function in or around primary cilia to make sure that they form correctly, keep their length and shape and that all of the signalling they are involved in occurs properly. Mutations in any of these proteins can disrupt their function and therefore affect primary cilia. This leads to a subset of diseases, which are together termed ciliopathies. One of these ciliopathies is Joubert syndrome. Joubert syndrome is a rare developmental disorder that is characterized by abnormal brain development and kidney and liver abnormalities. It is a genetic disease and all patient mutations identified to date are located in genes encoding proteins that are known to function in or around primary cilia. The core of a primary cilia is formed by a sophisticated structure, which is called the axoneme. The axoneme provides structural support to the cilium and is build up from microtubules. Microtubules are hollow cylindrical protein polymers consisting of α/β tubulin dimers, which causes them to have polarized ends. They are highly dynamic, constantly switching between shrinkage and growth. In cells this is regulated by microtubule associated proteins or 'MAPs'. The microtubules that make up the axoneme determine the length of the cilium. Ciliopathy patient-derived cells typically contain cilia with abnormal lengths, indicating that length is essential for cilia to function properly. The ciliary tip module is a group of five MAPs; ARMC9, CCDC66, CEP104, TOGARAM1 and CSPP1, which all locate to the tip of primary cilia where they regulate the length of the microtubules in the axoneme and therefore the length of the cilium. In this study we looked at how the proteins of the tip module bind to each other, as this could contribute to better understanding how they regulate microtubule length together. Mutations in all tip module proteins except from CCDC66 have been found in Joubert syndrome patients. We found that these mutations can inhibit tip module proteins to bind to each other, showing that interactions between these proteins are important and when disturbed can cause disease.

Uncropped and unprocessed western blots

Figure 1B

GFP – ARMC9 FL

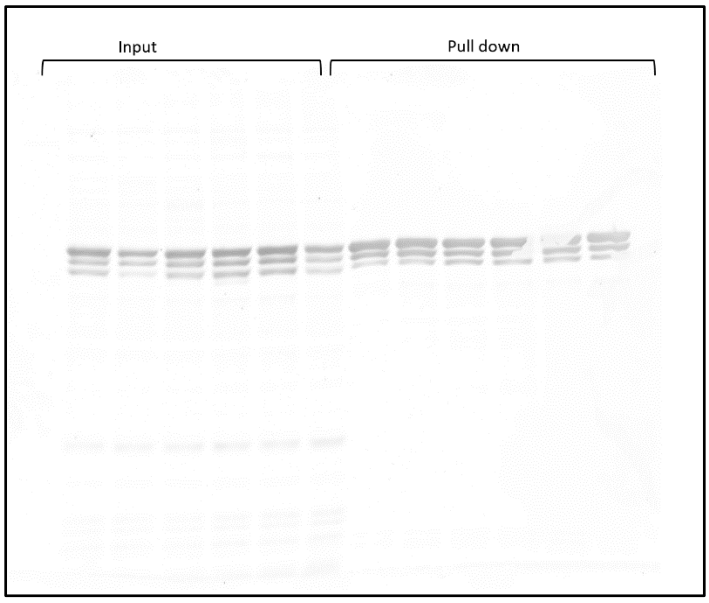

mCherry – tip module proteins FL

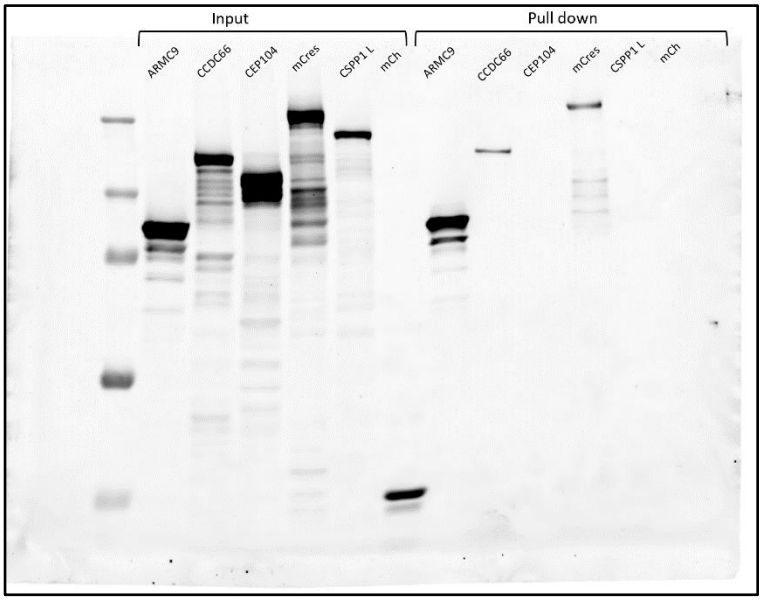

Figure 1C

GFP – CSPP1-s FL

mCherry – ARMC9 FL

Figure 2D

GFP – mCrescerin1

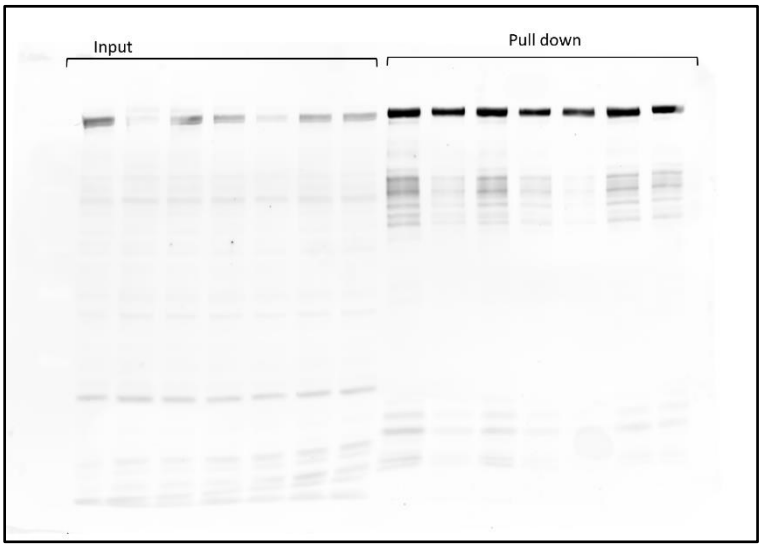

mCherry – ARMC9 constructs

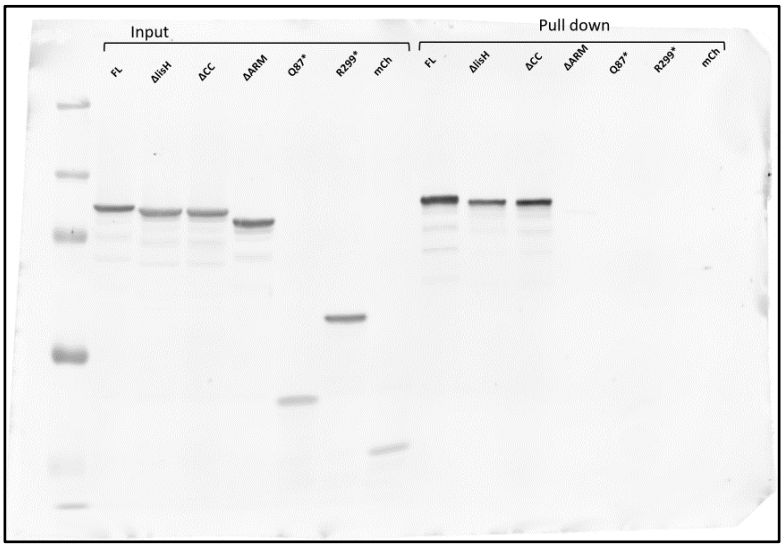

Figure 2F

GFP – ARMC9 FL

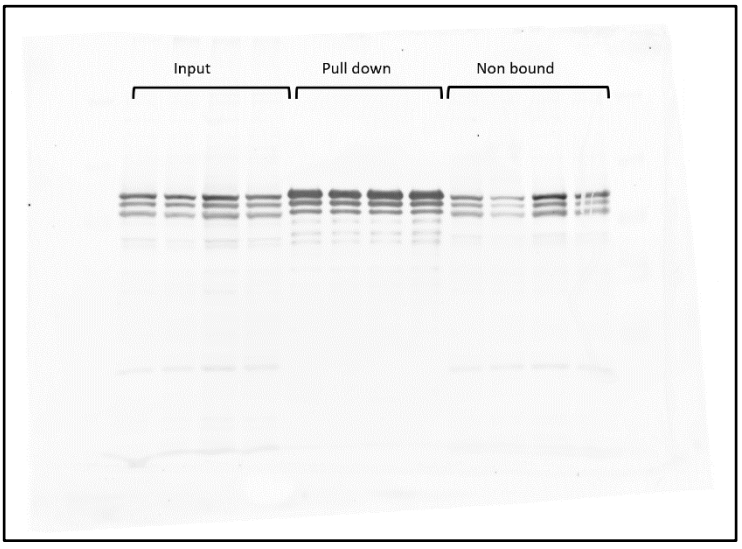

mCherry – mCrescerin1 constructs

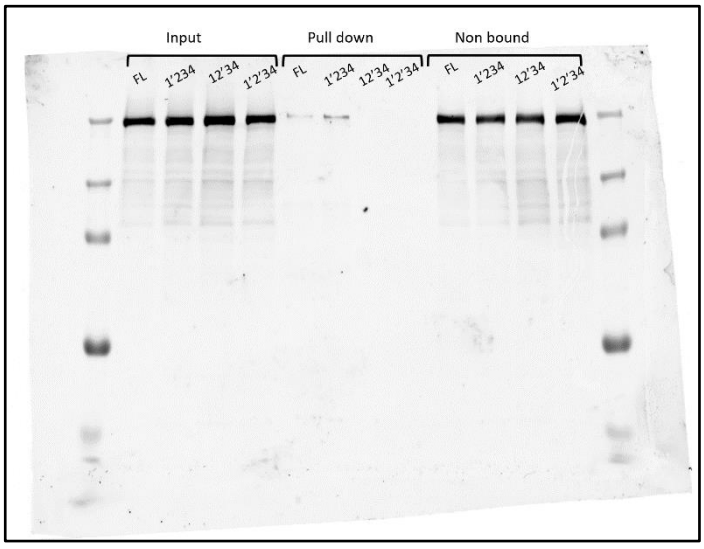

Figure 3B

GFP – ARMC9 FL

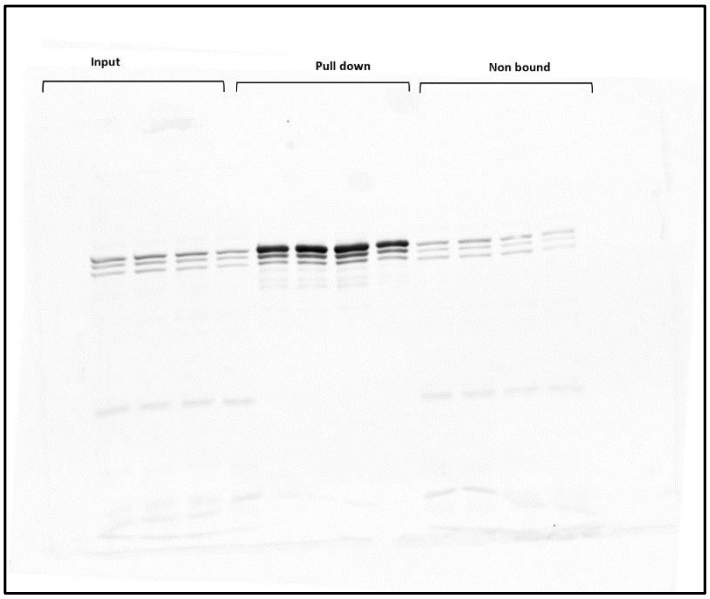

mCherry - mCrescerin1 constructs

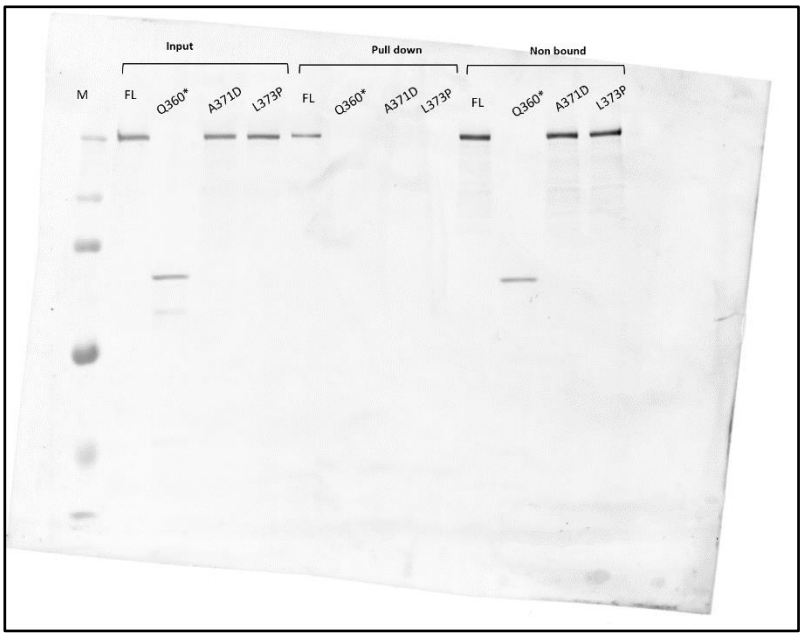

Figure 3C

GFP – mCrescerin1 FL

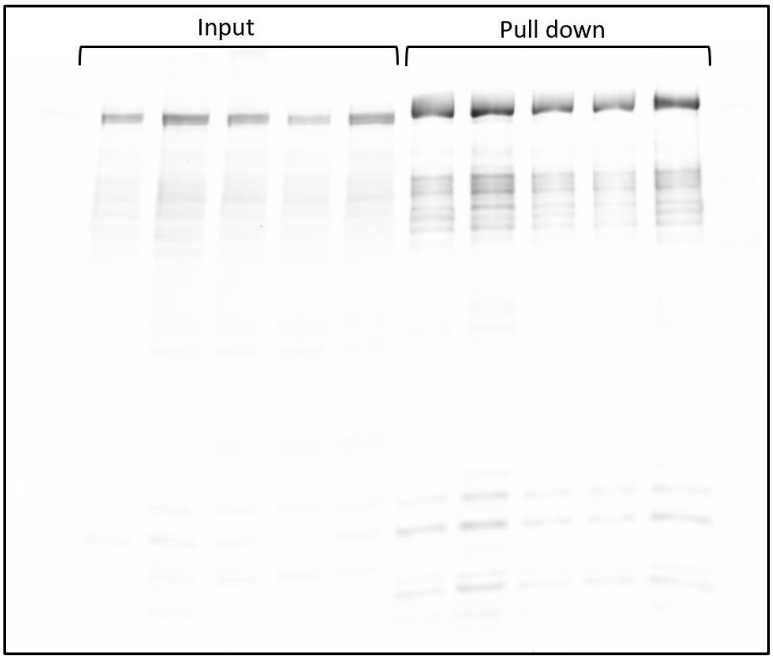

mCherry – ARMC9 constructs

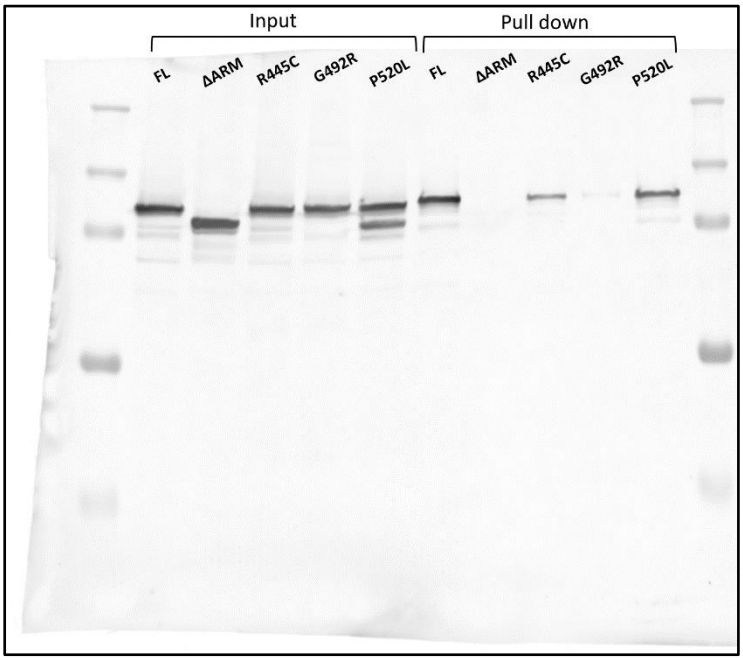

Figure 4A

GFP – CSPP1 short isoform FL

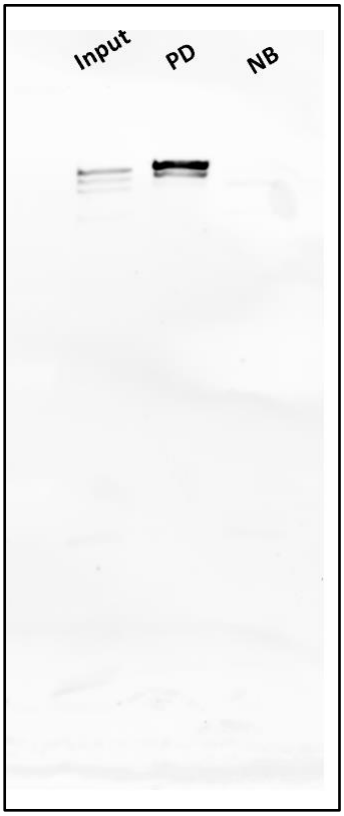

mCherry – mCrescerin1 FL

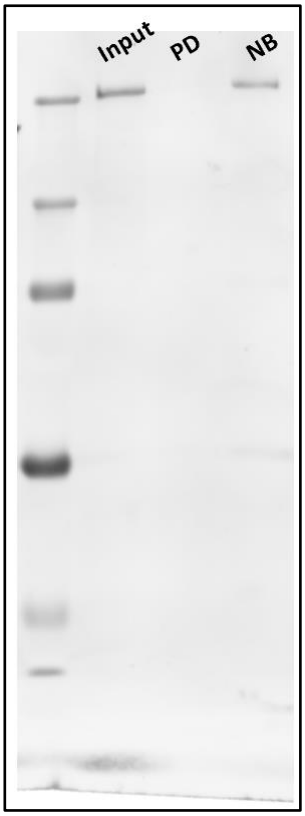

Figure 4B

GFP – CSPP1 short isoform FL

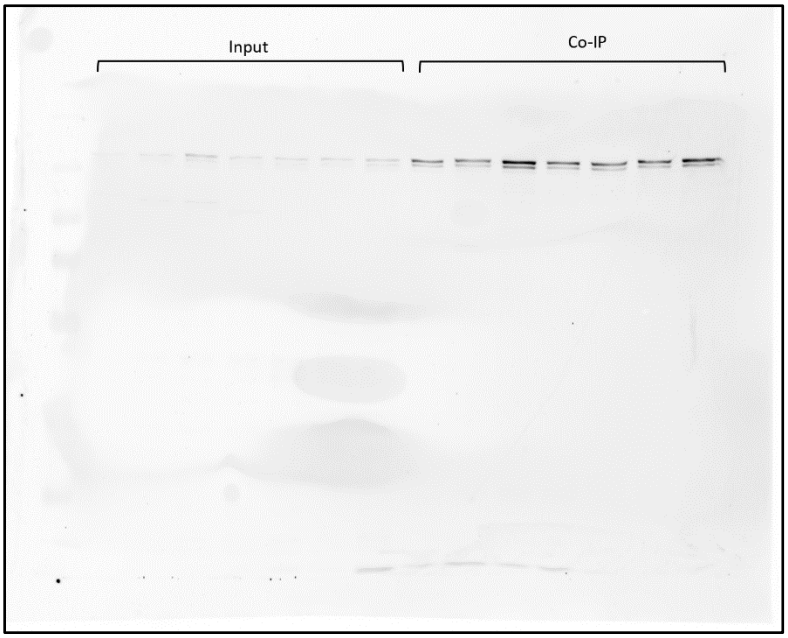

mCherry – ARMC9 constructs

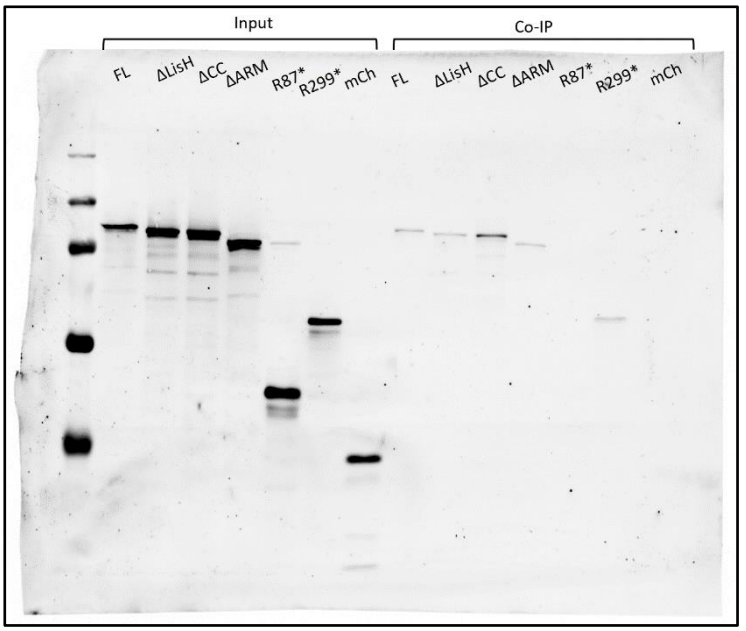

Figure 4C

GFP- CSPP1 constructs

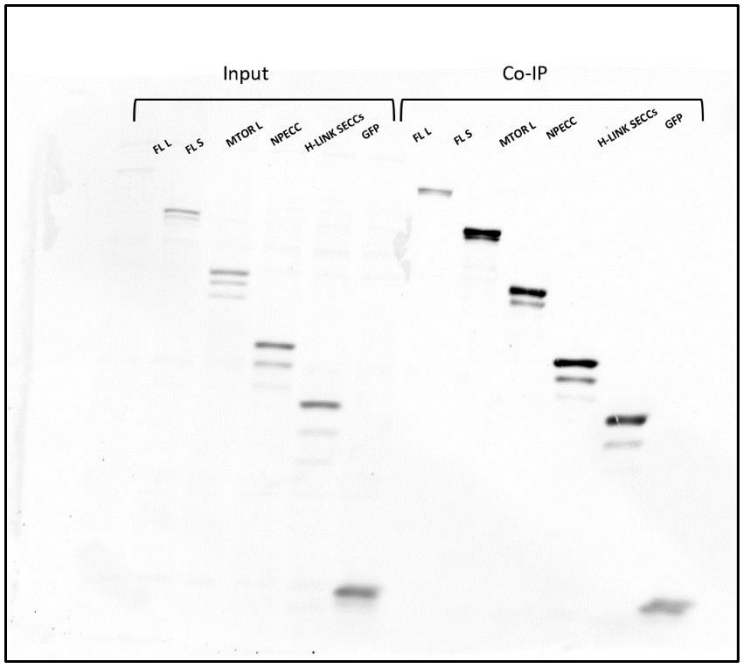

mCherry – ARMC9 FL

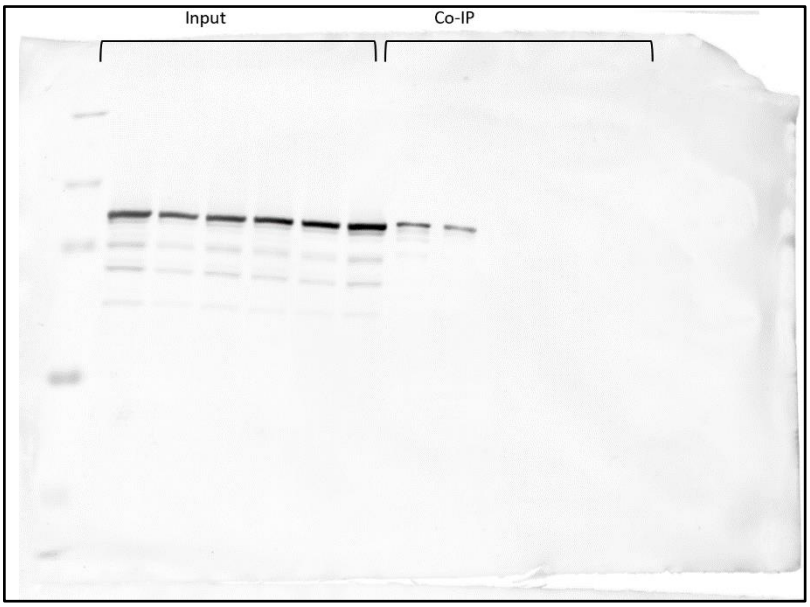

Figure 5C

GFP – CEP104 FL

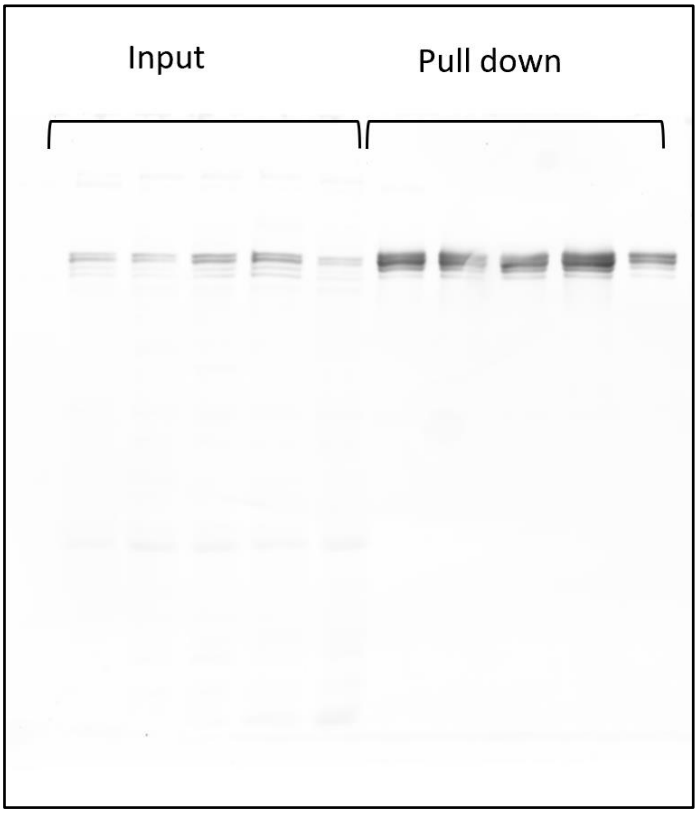

mCherry – mCrescerin1 constructs

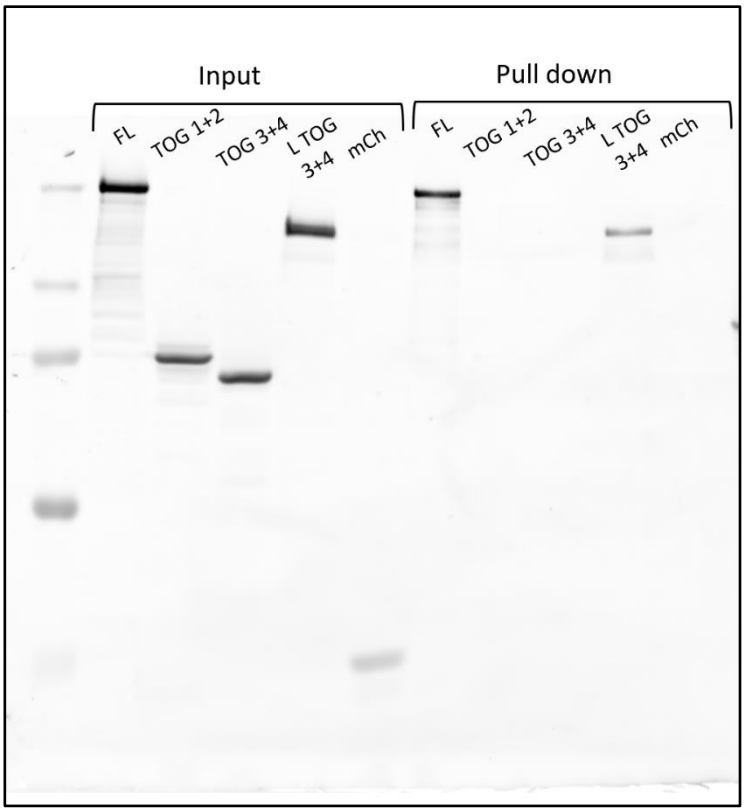

Figure 5D

GFP – mCrescerin1 FL

mCherry – CEP104 constructs

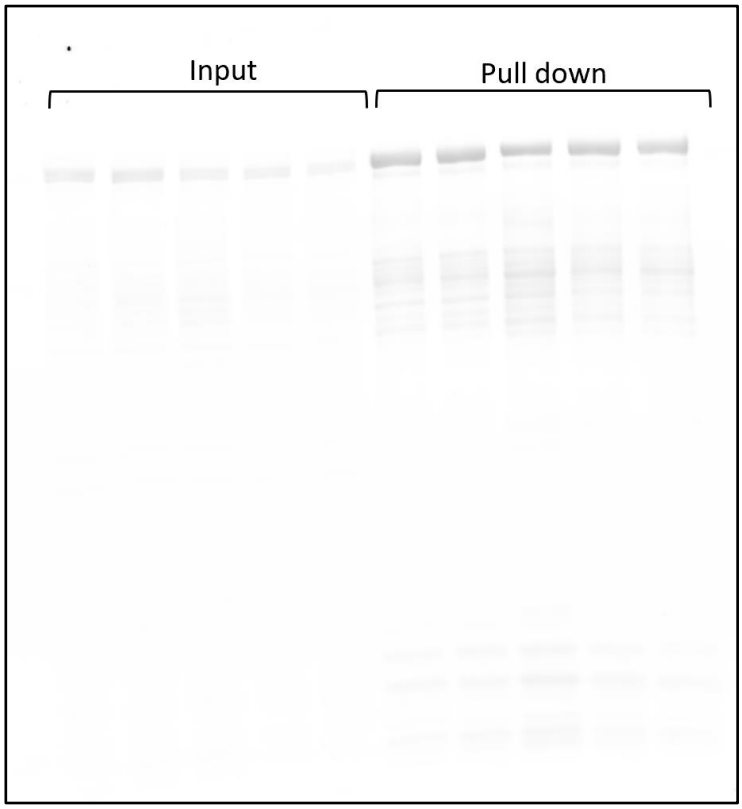

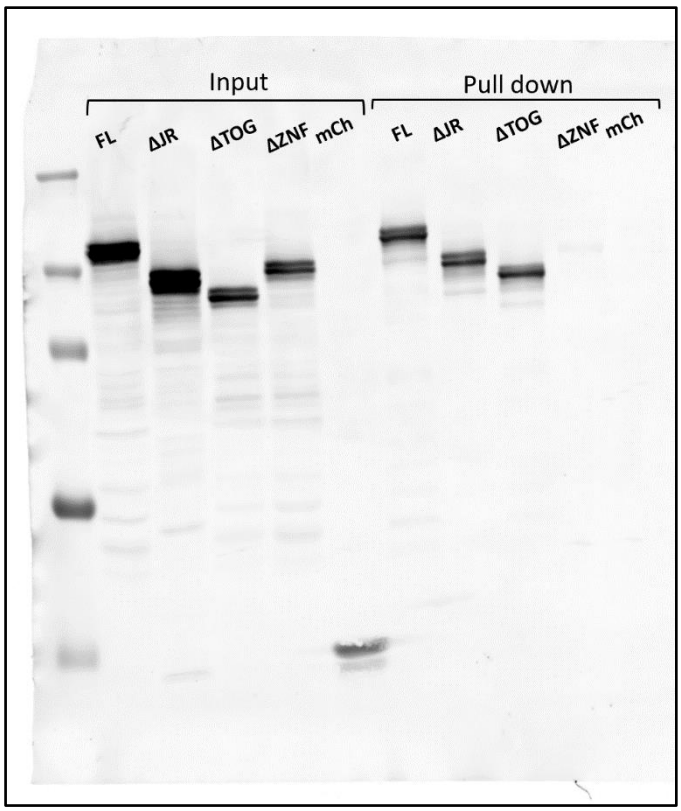

Figure 6D

GFP – CCDC66 FL

mCherry – CEP104 constructs

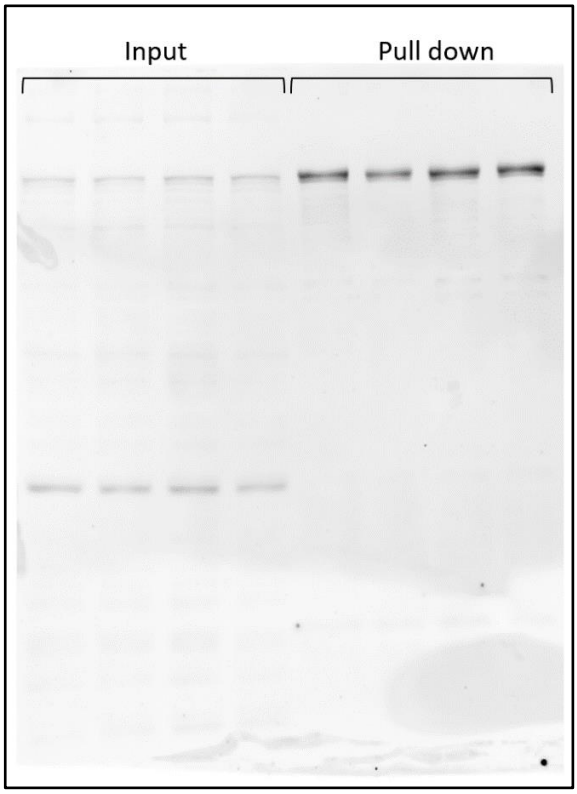

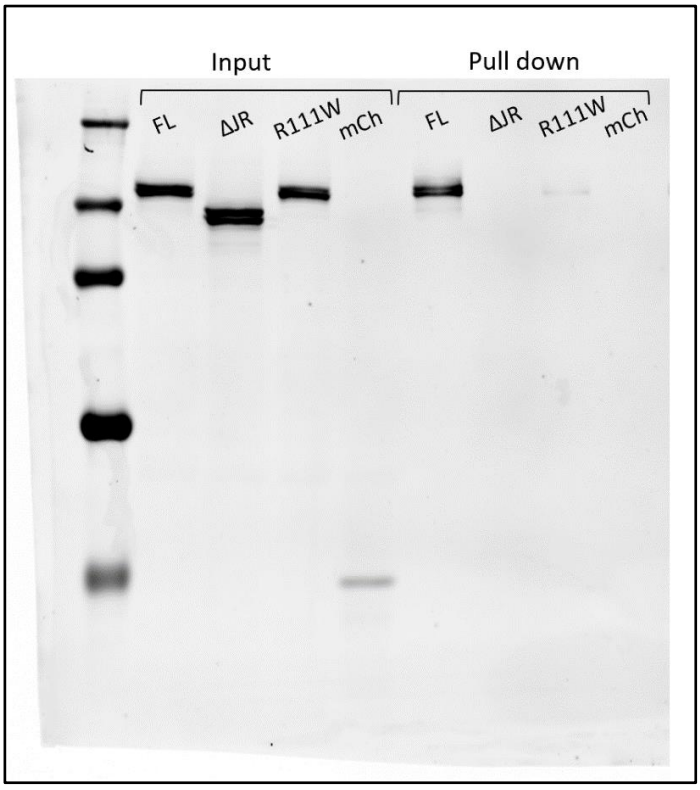

Figure 6E

GFP – CSPP1 short isoform FL

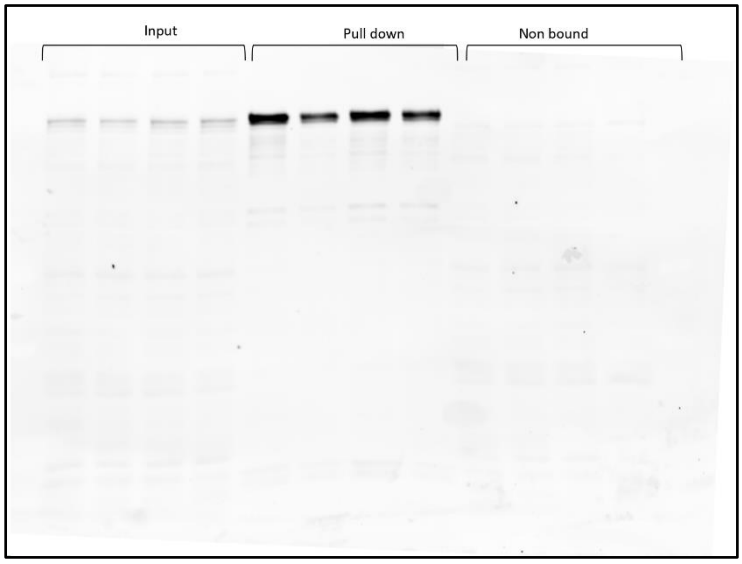

mCherry – CEP104 constructs

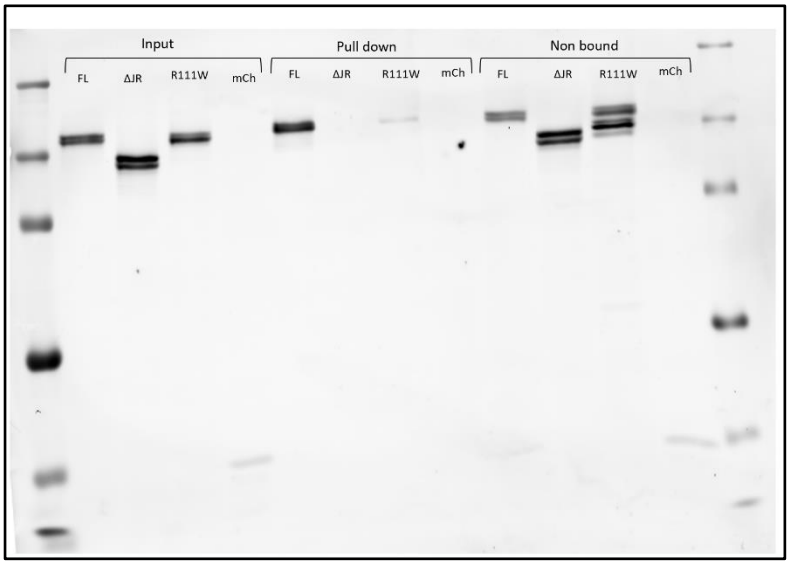

Figure S2B

GFP – ARMC9 FL

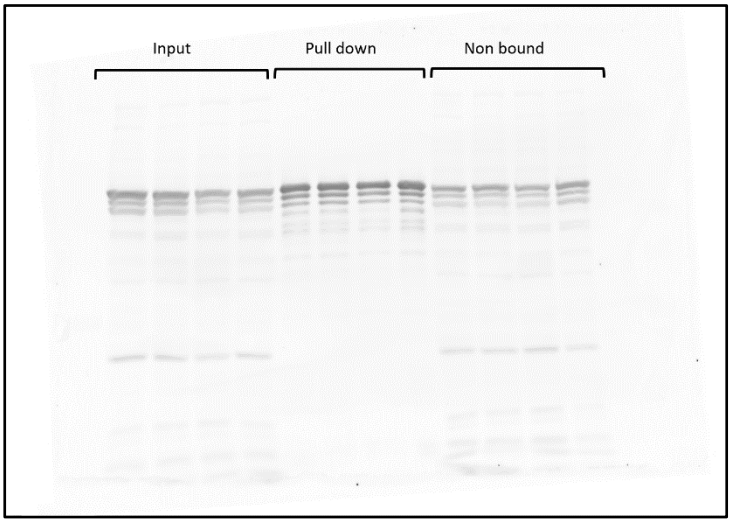

mCherry – mCrescerin1 constructs

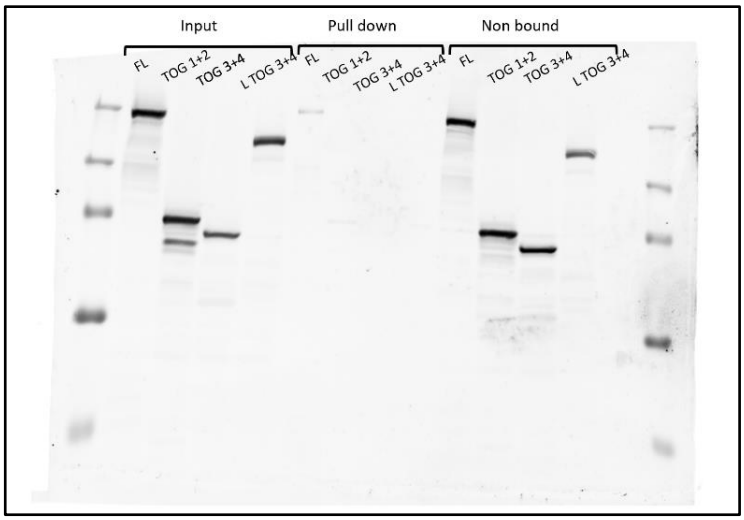

Figure S3B

GFP – mCrescerin1 FL

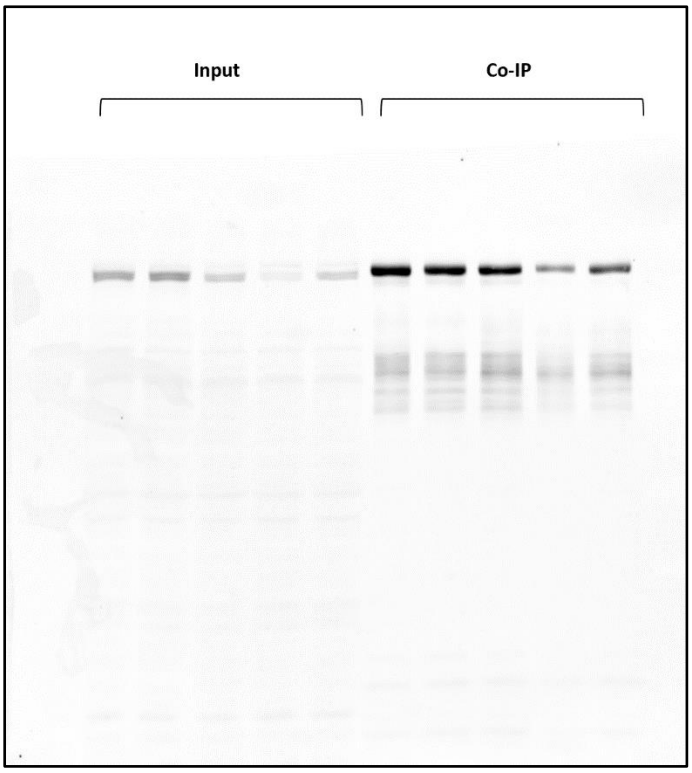

mCherry – CEP104 constructs